Universidade de Aveiro

Departamento de engenharia de materiais e cerâmica

2018

DAYANA L. GUZMAN SIERRA

BIONANOCOMPÓSITOS PIEZOELÉTRICOS FLEXÍVEIS PARA SENSORES BIOMÉDICOS

FLEXIBLE PIEZOELECTRIC BIONANOCOMPOSITES FOR BIOMEDICAL SENSORS

Universidade de Aveiro Departamento de Engenharia de materiais e cerâmica

2018

DAYANA L. GUZMAN SIERRA

BIONANOCOMPÓSITOS PIEZOELÉTRICOS FLEXÍVEIS PARA SENSORES BIOMÉDICOS

FLEXIBLE PIEZOELECTRIC BIONANOCOMPOSITES FOR BIOMEDICAL SENSORS

Dissertação apresentada à Universidade de Aveiro para cumprimento dos requisitos necessários à obtenção do grau de Mestre em materiais e dispositivos médicos, realizada sob a orientação científica da Doutora Paula Celeste da Silva Ferreira, Equiparada a Investigadora Coordenadora do Departamento de Engenharia de Materiais e Cerâmica da Universidade de Aveiro e da Doutora Cláudia Sofia Cordeiro Nunes, Pós- Doutoranda do Departamento de Engenharia de Materiais e Cerâmica da Universidade de Aveiro.

Este trabalho foi desenvolvido no âmbito do projeto CICECO-Aveiro Institute of Materials POCI-01-0145-FEDER-007679 (Refª. FCT UID/CTM/50011/2013); do projeto NANOTRONICS (IF/300/2015); e do projeto FLEXIDEVICE (PTDC/CTM-CTM/29671/2017) financiados por fundos nacionais através da FCT/MEC e quando aplicável cofinanciado pelo FEDER, no âmbito do Acordo de Parceria PT2020. Agradece-se também ao projeto co-promoção Smart Green Homes (POCI-01-0247-FEDER-007678) financiado pelo P2020, no âmbito do Programa Operacional Competitividade e Internacionalização, e pelo FEDER.

A mi familia.

O júri

Presidente	Prof. Doutor Pedro Manuel Lima de Quintanilha Mantas professor auxiliar do Departamento de Engenharia de Materiais e Cerâmica da Universidade de Aveiro
Arguente	Prof. Doutor Luis Manuel Cadillon Martins professor associado C/ Agregação da Faculdade de Física da Universidade de Aveiro
Orientadora	Doutora Paula Celeste da Silva Ferreira equiparada a investigadora coordenadora do Departamento de Engenharia de Materiais e Cerâmica da Universidade de Aveiro

Acknowledgements First, I would like to thank my supervisors Dr. Paula Ferreira and Dr. Claudia Nunes for the challenge and the opportunity to be part of this research, for guide me with patience and for sharing their knowledge and positivity in this project.

I also want to thank to:

- Dr. Rosário Soares from *Laboratório Central de Análises* of University of Aveiro for helping me with XRD characterization, MSc. Celeste Azevedo from the chemical department of University of Aveiro for her support with Raman Analyses, Eng. Marta Ferro and Eng. Tiago for their help in SEM and Dr. Igor Bdikin from department of Mechanics for his detailed support in PFM analyses.
- My laboratory colleagues Zélia, Ana, Mariana, Joana and Fernando (Thank you for your help and support with doubts and processes).
- The Electroceramics group for received me, especially to Dr Oleksandr Tkach, Dr. Olena Okhay and Rui Pinho for their availability and help along this project.
- Prof. Paula M. Vilarinho for her advice and her indirect way of motivating students to be part of the world of science.
- My friends and family for supporting me and giving me the strength to continue.
- And, finally, Aveiro.

"Those who pass by us, do not go alone, and do not leave us alone; they leave a bit of themselves, and take a little of us." Antoine de Saint-Exupéry.

Palavras-chave Bionanocompósitos, titanato de bário, quitosana, piezoeletricidade, sensores.

Resumo

Nas últimas décadas, tem havido um interesse crescente no desenvolvimento de novos materiais com o intuito de alcançar a "Internet of Things (IoT)" que prevê a ligação de 20 a 30 bilhões de dispositivos à internet até 2020. A implementação da “Internet of Things” exige o desenvolvimento de tecnologia base, onde se incluem os dispositivos de captação de energia, atuadores e sensores. Os sensores são muitas vezes utilizados em aplicações biomédicas que exigem flexibilidade, biocompatibilidade e sustentabilidade. Neste contexto, a motivação deste trabalho foi a preparação de um bionanocompósito para sensores piezoelétricos biocompatíveis para aplicações biomédicas. Assim, escolheu-se como matriz um polissacarídeo que tem a capacidade de formar películas (filmes) facilmente, e partículas de titanado de bário que é um material ferroeléctrico e piezoeléctrico à temperatura ambiente, não possuindo chumbo na sua composição.

As partículas de $BaTiO_3$ foram sintetizadas por método hidrotermal a temperatura moderada (200 °C) e na ausência de solventes orgânicos. Foram estudadas vários tempos de reação de forma a selecionar as condições ideais para a preparação das partículas com as propriedades adequadas para a incorporação nos filmes à base de quitosana. A caracterização estrutural por difração de raios-X (DRX) e espectroscopia de Raman permitiu verificar que as partículas sintetizadas a 200 °C apresentavam, ao fim de 24 horas de síntese, a estrutura cristalográfica tetragonal bem definida. As partículas mostraram morfologia cúbica uniforme e tamanho médio de cerca de 306 nm. Em geral, os tamanhos das partículas e de cristalites aumentam com o tempo de reação. Os filmes foram obtidos pelo método de evaporação de solvente, após a dispersão das partículas, em diferentes proporções, numa solução de quitosana. As propriedades estruturais (DRX) e morfológicas (SEM); físico-químicas (mecânicas, grau de humidade, solubilidade em água e ângulo de contacto e Raman); e elétricas (comportamento dieléctrico, curvas de histerese e resposta piezoelétrica à escala nanométrica) dos filmes foram caracterizadas. A adição de partículas melhorou as características mecânicas dos filmes de quitosana, tornando-os mais resistentes, elásticos e dúcteis. Estes filmes revelaram também serem mais resistentes à água, o que revela que existe uma interação entre as partículas e a matriz de quitosana. Em relação ao comportamento elétrico dos filmes, o aumento de partículas melhora a permitividade das amostras cinco vezes em relação ao material biopolimérico. Foi verificada uma grande dificuldade de deposição de elétrodos nos filmes flexíveis que se pode justificar com base nas características das amostras e/ou na inadequação das condições experimentais de deposição dos elétrodos na amostra. Como não foi possível medir a resposta piezoeléctrica à escala macroscópica, nem polarizar uma área da amostra de bionanocompósito, fez-se o estudo da resposta piezoelétrica à escala nanométrica por microscopia atómica de resposta piezoelétrica. Os filmes com a concentração mais elevada de nanopartículas mostraram claramente domínios piezoelétricos, não sendo, contudo, possível traçar uma curva de histerese aceitável nem polarizar uma pequena área do nanocompósito. Esta observação, juntamente com a análise por microscopia de potencial de superfície do filme controlo (só de quitosana) que indica a presença de cargas no polímero puro, leva à conclusão da existência de um comportamento do tipo electret pelo que será necessário encontrar uma estratégia para eliminar (ou reduzir) a contribuição da matriz.

Apesar das dificuldades encontradas, os bionanocompóstos desenvolvidos, à base de quitosana e titanato de bário são promissores para serem usados em dispositivos biomédicos (por exemplo em compressas para libertação de fármacos, etc.) devido à sua elevada resistência mecânica, elasticidade e ductilidade, sendo adaptados a condições de elevado grau de humidade. Estes bionanocompósitos são ainda biocompatíveis e parcialmente biodegradáveis, tendo potencial para serem usados como alternativa aos polímeros sintéticos.

Key words Bionanocomposite, barium titanate, chitosan, piezoelectricity, sensor.

Abstract

In recent decades, there has been increasing interest in the development of new materials in order to achieve the "Internet of Things (IoT)" which provided for the connection of 20 to 30 billion devices to the Internet by 2020. The implementation of the "Internet of Things "requires the development of base technology, which includes transducers, actuators and sensors. Sensors are often used in biomedical applications that require flexibility, biocompatibility and sustainability. In this context, the motivation of this work was the preparation of a bionanocomposite for biocompatible piezoelectric sensors for biomedical applications. Thus, a polysaccharide that have the ability to form films (films), and particles of barium titanate which is ferroelectric and piezoelectric material at room temperature, having no lead in its composition.

The BaTiO3 particles were synthesized by hydrothermal method at moderate temperature (200 °C) and in the absence of organic solvents. Several reaction times were studied in order to select the ideal conditions for the particles preparation with the required properties to be incorporated in the chitosan-based films. The structural characterization by X-ray diffraction (XRD) and Raman spectroscopy allowed us to verify that the particles synthesized at 200 °C showed a well-defined tetragonal crystallographic structure after 24 hours of synthesis. The particles showed uniformed cubic morphology and average size of about 306 nm. In general, particle and crystallite sizes increase with reaction time. The films were obtained by the solvent evaporation method, after dispersing the particles in different proportions, in a solution of chitosan. Structural properties (XRD) and morphological (SEM); physical-chemical (mechanical, degree of humidity, solubility in water and contact angle, and Raman); and electrical (dielectric behavior, hysteresis curves and nanoscale piezoelectric response) of the films were characterized. The addition of particles improved the mechanical properties of the chitosan films, making them more resistant, elastic and ductile. These films have also been shown to be more resistant to water, which reveals that there is an interaction between the particles and the chitosan matrix. In relation to the electric behavior of the films, the increase of particles improves the permittivity of the samples five times in relation to the biopolymer material. It was verified a great difficulty of deposition of electrodes in the flexible films that can be justified on the basis of the characteristics of the samples and / or the inadequacy of the experimental conditions of deposition of the electrodes in the sample. It was not possible to measure the piezoelectric response at the macroscopic scale nor to polarize an area of the bionanocomposite sample. Thus, the piezoelectric response at the nanometric scale was studied by atomic microscopy of piezoelectric response. It was found that nanocomposite films with the highest concentration of nanoparticles clearly showed piezoelectric domains, but it is not possible to obtain an acceptable hysteresis curve and to polarize a small area of the nanocomposite. These observations, together with the analysis by surface potential microscopy of the control film (chitosan only) that indicates the presence of charges in the pure polymer, lead to the conclusion of an electret type behavior, being necessary a strategy to eliminate (or reduce) the matrix's contribution.

Despite the difficulties encountered due to degree of innovation of the work, the bionanocomposites developed based on chitosan and barium titanate are promising to be used in biomedical devices (drug release pads, etc.) since they have high mechanical resistance, elasticity, and ductility, as well as have higher resistance to conditions with high degree of humidity. In addition, they are biocompatible and partially biodegradable, being an excellent alternative to synthetic polymers.

Table of Contents

Index of Figures

Index of Tables

List of symbols

d_{33}	Direct piezoelectric constant
$BaCl_2$	Barium Chloride
$BaTiO_3$	Barium Titanate
D_{SEM}	Main size of particles measured by SEM
D_{XRD}	Main size of crystallite measured by X-ray diffraction
E	Electric field
ε_0	Permittivity of vacuum
ε_r	Relative permittivity
ε'	Real permittivity
ε''	Imaginary permittivity
f	Frequency
NaOH	Sodium hydroxide
P	Polarizability
P	Probability
S	Strain
St	Stress
σ	Conductivity
tan δ	Dielectric loss
T*c*	Curie temperature
TiO_2	Titanium dioxide
Y	Young modulus
Z	Impedance

List of Abbreviatures

a.u.	Arbitrary units
BT	Barium titanate
Eq	Equation
EB	Elongation at break
f-PEH	Flexible piezoelectric energy harvester
FT-IR	Fourier transform infrared
FWHM	Full-width at half maximum
H	Hydrated
KFM	Kelvin probe force microscope
LO	Longitudinal orientation
nH	Non-Hydrated
NPs	Nanoparticles
PDMS	Polydimethylsiloxane
PFM	Piezoresponse force microscopy
PVDF	Polyvinylidene fluoride
PZT	Lead zirconate titanate
ROHS	Restriction of Hazardous Substances
SEM	Scanning Electron Microscope
TO	Transversal orientation
TS	Tensile strength
XRD	X-ray diffraction

Chapter 1

1.1 Objective

The main goal of this dissertation is to:

Develop a flexible piezoelectric bionanocomposite material based on chitosan with barium titanate particles ($BaTiO_3$) to be integrated into the fabrication of a sensor for biomedical applications.

The specific objectives are:

(i) Synthesis and characterization (structural and physical-chemical) of $BaTiO_3$ nanoparticles (NP) obtained by the hydrothermal method;

(ii) Preparation of bionanocomposites films based on chitosan with different concentrations of $BaTiO_3$ NP by solvent casting;

(iii) Physical-chemical characterization of the obtained composite films and study of their piezoelectric response.

1.2 Structure of the dissertation

This dissertation is divided into six chapters. The first chapter is a preamble of the document including objectives and the way the thesis is divided. The second chapter contains the state of art with the concepts and processes considered relevant to understand the research project developed. Chapter 3 is dedicated to the description of the experimental procedures for materials synthesis and characterization. Chapter 4 joins the results and discussion on the synthesis of barium titanate particles. The fifth chapter contains the results and discussion concerning the development of chitosan-based films and their characterization. The last chapter integrates the conclusion and proposes potential future lines of research.

Chapter 2 Introduction

Among the last years, an increasing interest in novel systems for biomedical applications has been identified[1], [2]. The search for new materials for the fabrication of more comfortable, efficient, and reliable devices to monitor and regulate different parameters in the body leads to the creation of sensors[3]. The conventional electronic systems based on hard and brittle materials are not viable due to the requirement of large mechanical deformation and the urgency for more environmentally friendly, sustainable, long lasting and remote use devices. This challenge has driven to the production of a wide range of functional structures that allow to obtain more efficient accurate, rapid and reliable information[4].

The crescent applications of the *Internet of Things* (IoT) concept and the integration of biomedical sensors into wearable devices have enhanced the interest and research of novel materials and interfaces to interact with human body[5]. Flexible and transparent smart systems have been intensively researched by the scientific community and by several companies[2], [6]. This technology allows the integration of innovative products making use of different aspects of the applied materials and compounds[1]. It is already available for consumers in a wide range of innovative products, e.g. flexible displays, radio-frequency identification tags, and wearable electronic skins, which could collect and analyze data for medical applications[7], [8].

Since the creation of the first flexible piezoelectric energy harvester (f-PEH) in 2006, the production of different alternatives that use nanocomposites materials, as zinc oxide (ZnO), lead zirconate titanate (PZT), or barium titanate ($BaTiO_{3)}$, over a polymeric matrix have been documented[9]. The novel structures have been created not just to sense a behavior but to work as the overall system power supply. Smart patches and tattoos are examples of the new wearable developed technologies[10]. Due to the European directive for restriction of certain hazardous substances (RoHS) in electrical and electronic equipment, published in 2003, one of the main challenges is to develop more environmentally friendly and non-toxic structures, thus the development of bionanocomposites using low temperatures techniques has been widely studied.[11]

This chapter attempts to introduce the main concepts and state of art of bionanocomposites for biomedical sensors. First, a general definition and required parameters for biomedical

sensors are addressed. Furthermore, the materials used for this kind of applications are reviewed. Bionanocomposite concept and its properties are studied to introduce one of the main components of this research, chitosan, followed by the study of the piezoelectric phenomena, and ferroelectricity to introduce the lead-free ceramic barium titanate properties. Finally, the main processes to obtain a flexible bionanocomposite thick film are described.

2.1 Biomedical sensors

According to the Instrument Society of America, a biomedical sensor is a transduction device that transforms a measurable quantity or parameter into an electrical signal that could be processed and digitalized[12]. It permits the quantification of biophysical processes to be utilized in the prevention, diagnosis, and monitoring of diseases or treatments in health and well-being fields.

Taking into account the classification of the instrumentation, transductors could be of measurement or control (feedback)[1]. In this second case, they act as actuators, generating a response that modifies some activity in the system they belong. The sensors are monitoring and measurement devices. In the human body there are several variables that could be measured, as temperature, heartbeat or pressure. Depending on the measured variable, the sensor can be classified in mechanical (position, displacement, force, acceleration, pressure, flow rate, rpm, acoustic waves, etc.), thermal (temperature, heat flow, etc.), electrostatic, radiation (electromagnetic, nuclear, etc.), chemical (concentration of humidity, gas components, ions, etc.) and biological (concentration of enzyme substrates, antigens, antibodies, etc.)[13]. The electrical signals have been the most used, considering the facility for processing and analysis[1],[7].

The sensors could be modulator or generator, in relation to the source. The research in wearable technology requires the implementation and miniaturization of integral systems. Consequently, sensors which do not need a source to work (generator) have increased their popularity in the flexible electronics field [2], [8], [14].

A sensor has three levels that should be taken in consideration in the fabrication process. In the first level the sensor can show an output signal with a balanced offset and a compensated temperature effect; in the second level, signal amplification is done and in the last stage the incorporation of a microprocessor or memory is implemented for a specific application[1].

The expected properties to produce the first biomedical sensors where related to a good linearity, low hysteresis and offset values, low temperature effects, low interference, high signal-noise relation, good interchangeability, high lifetime, stability and reliability. Nevertheless, new challenges associated to miniaturization and integration to portable and connected systems add more properties, such as flexibility, stretch ability, and biocompatibility.

Applications are wide and the main action fields are monitoring and mapping of parameters in real time for diagnosis, tracking, and prevention of diseases. These devices not only include sensors but also actuators for parameter control in users. Depending on the future use of the sensor there will be a list of requirements that have to be accomplished, for instance, continuous monitoring of physical parameters, as temperature and strain, for small applications in clinic diagnosis (Figure 2.1).

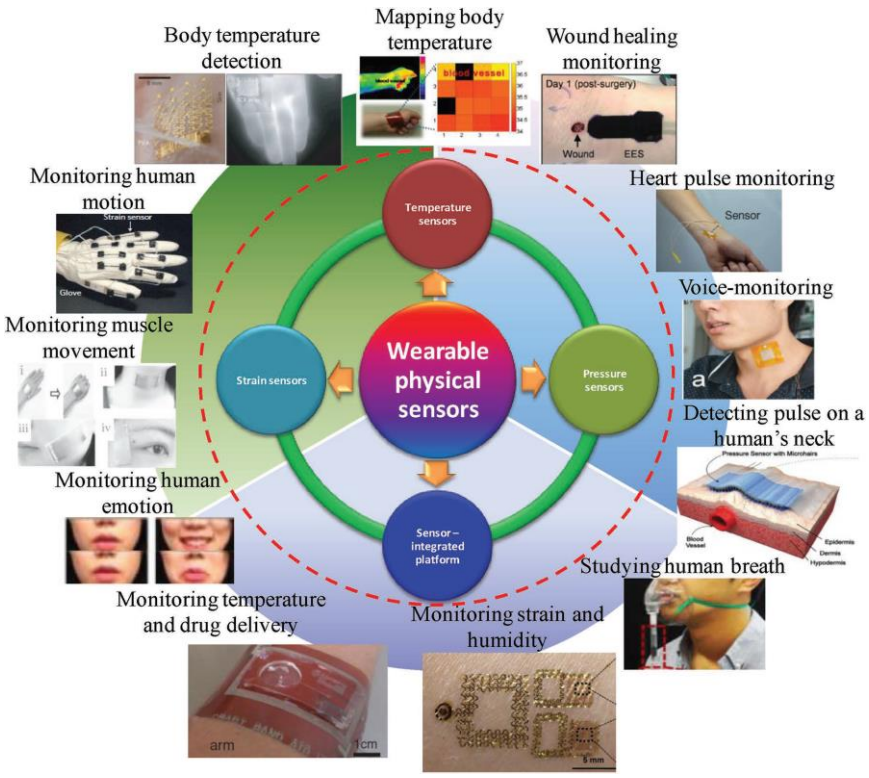

Figure 2.1 Possible applications of physical flexible sensor.[2]

Stretchable physical sensors possessing unique characteristics such as ultrathin, elasticity, lightness and high flexibility, are currently a wide research field driven by the need of more reliable devices for body signal detection and monitoring adaptable to different organ surfaces and capable of enhancing the human well-being[2], [15].

2.2 Materials for biomedical sensors

Over the last years, the materials that have been used for piezoelectric sensor fabrication changed according to their response to sensing phenomena. Commonly used materials for biomedical sensors included single crystals as quartz, silica, and another semiconductor compounds. They showed many advantages such as low cost production, possibility of miniaturization with low charge consumption and easiness of integration into other electronic systems. The need of miniaturization together with the performance dependence on temperature and composition, lead to the implementation of polycrystalline materials

like ceramics especially the lead-oxide based ABO_3 perovskites (PZT) due to their excellent piezoelectric properties for sensors and actuators[16]. Some polymers like polyvinylidene fluoride (PVDF) and polydimethylsiloxane (PDMS) are also widely studied and used for sensor fabrication[14], [17], [18].

2.2.1 Properties of bionanocomposites for biomedical sensors

Composites comprise the blend of two or more materials with notable differences in their physical and chemical properties. In general, they are developed to enhance the properties of each material trying to find a balance between the advantages and disadvantages to develop a specific application. Bionanocomposites, also known as green biohybrid composites, include two groups of materials: organic species (mainly biopolymers) and inorganic solids at nanometer scale embedded into it.[19] They contrast with nanocomposites in preparation method, properties, functionalities, biocompatibility, biodegradability, and applications.[20] The use of biopolymers as raw materials has been a crescent topic of interest in the last decade due to their environmental friend features.[21]

Despite the high piezoelectric response of PZT, the lead content in its structure is an environmental concern. Alternative lead-free ferroelectrics as $BaTiO_3$ (with a high permittivity constant) have been attracting the attention of researchers. Figure 2.2 displays the growing trend of the Web of Science number of citations with the keywords “lead-free” or “barium titanate” since the year 2000.[22]

The attempt to build flexible and functional structures found in polymer-based composites the required characteristics to reach these goals due to the useful dielectric performance, low dielectric losses, low cost and processing easiness of the polymeric matrices.[23] Biopolymers like chitosan and alginate have been proposed and explored for these applications considering its abundance on nature, mechanical properties, and chemical stability[24].

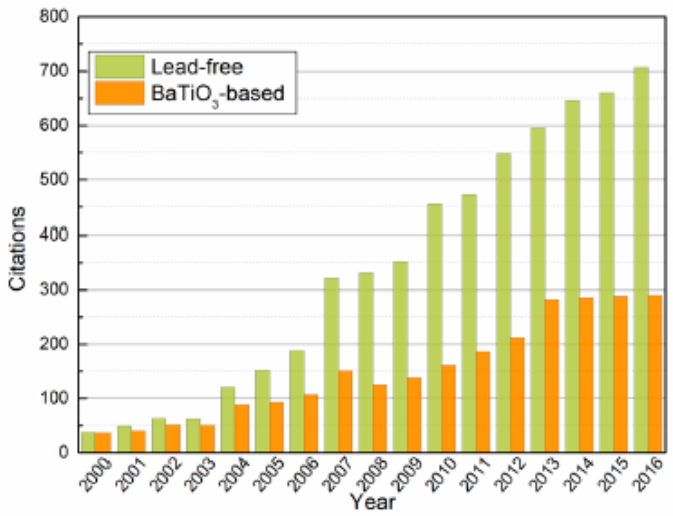

Figure 2.2. Lead free and $BaTiO_3$ citations in the last years Gao,J, *et al*[22].

Table 2.1 shows literature examples of the application of nanocomposites for different sensor applications. PVDF is the most commonly used polymer for piezoelectric applications due to its larger piezoelectric coefficient in comparison with other polymers (20-28 pC/N) and has been also tested as a matrix for different nanoparticles as barium titanate and Zinc oxide to enhance its properties. Related to the application, the materials have been projected for the production of nanogenerators for micromechanical systems and also as vibration sensors and actuators.

Table 2.1 Lead-free piezoelectric sensors

Material application	nanocomposites	Reference
f-PEH	PZT	[25]
f-PEH	$BaTiO_3$-Resin hybrid film	[26]
Thin-film transistor	ZnO- Polymers substrate	[27]
Mechanical sensor	$BaTiO_3$-Chitosan electret	[28]
f-PEH	$BaTiO_3$ nanotubes/PDMS	[29]
f-PEH	$BaTiO_3$-PVDF	[30]
Flexible sensor	$BaTiO_3$- Alginate	[31]
Piezoelectric thin film for fetu's heart	PVDF	[32]

Bionanocomposites show great mechanical properties, biocompatibility and biodegradability[11]. Nanocomposite antimicrobial systems are mostly successful due to the high surface to volume ratio and elevated surface reactivity of the nano-sized antimicrobial agents. These characteristics are of huge importance in regenerative medicine and in the development of environmental friendly materials[10], [33].

Another important attribute of medical biomaterial is biocompatibility, which is the capability to function properly in the human body to generate desired clinical outcomes, without causing hostile effects. Bionanocomposites are continuously utilized for biomedical applications[1], like drug delivery system[34], vaccination, wound dressings[35], and tissue engineering. The main advantages of these substances are biocompatibility due to their innate non-toxicity. Polymers reinforced with engineered or functional nanostructures offer supplementary optical, electrical, electromagnetic shielding and magnetic characteristics, which leads to the development of a variety of advanced devices: light emitting diodes, solar cells and display panels, sensors and other medical devices[33], [34], [36].

Additionally, the nanofillers can have the capacity to enhance the mechanical, thermal and barrier characteristics of the bionanocomposites and show other required functions.

2.2.2 Polysaccharide based bionanocomposites

Polymers are materials suitable for many practical applications due to their easy processability into flexible films.[37] Polysaccharides are emerging compounds in biomedical applications because they are biodegradable, water soluble, and have biological activities.[38], [39] Polysaccharides for such applications are available from diverse sources, including agricultural and marine resources. The potential for biomedical uses of polysaccharide-based materials can be enhanced by their chemical modifications to achieve the required functional activities for specific purposes[40].

2.2.2.1 Chitosan

Chitosan results from the deacetylation of chitin, needing to have more than 50% of deacetylation. Chitin is found in the exoskeleton of crustaceans such as crabs and shrimps, and some insects and is the second most plentiful biomass after cellulose. It is a linear polysaccharide composed of ß(1-4) linked D-glucosamine with randomly dispersed N-

acetyl-D-glucosamine groups. The structural composition of chitin and chitosan are showed in Figure 2.3[41]. Chitosan is a cationic polymer with semi-crystalline properties. The high charge density allows chitosan to be soluble below pH 5 and insoluble above pH 7. At high pH solutions, chitosan can be gelled into strong fibers and can be processed as membranes. [42] Its unique properties, such as biocompatibility, biodegradability and antibacterial capacity [41] make it attractive for many industrial and biomedical applications, including hemodialysis membranes, artificial skin, hemostatic agents, hemoperfusion columns, and drug delivery systems. Due to its pH dependent solubility, it forms stable films on various surfaces under neutral and basic pH conditions.

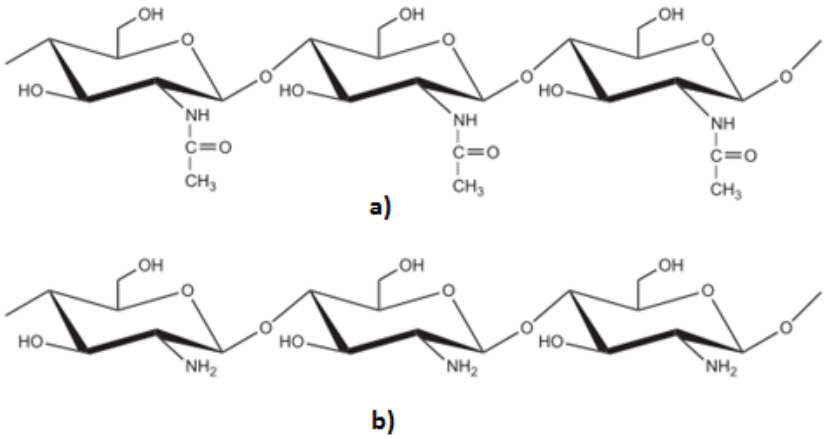

Figure 2.3 Chemical structure of a) chitin and b) chitosan.[41]

The main role of chitosan in the microdevices is to immobilize biomolecules, cells, or nanoparticles (NPs). This enables the devices to perform advanced functions. Perhaps, the most important property of chitosan is its ability to be modified with other substances improving functionality according to the material purpose. For instance, the addition of carbon nanotubes allows to obtain composite films with improved mechanical strength and conductivity. Another approaches, substances and objectives are described in the literature[43]

2.2.3 Piezoelectricity

Piezoelectricity was discovered in 1880 by Pierre and Paul-Jacques Curie in some materials, as quartz, tourmaline and Rochelle salt[44]. The prefix *piezo* was taken from the

Greek word *Piezein* that means *pressure,* thus, piezoelectricity is the property of some materials that allows the production of an electric charge or voltage in response to mechanical forces or stress and also the mechanical stress produced by an applied electric field[37]. This behavior is also related to the classification of the piezoelectric material as smart materials[16].

Crystals are divided into 32 classes called point groups depending on their orientation. These points are defined with respect to the origin of symmetry using the x, y and z coordinates. To exhibit piezoelectricity, the crystal should belong to one of the 20 non-centrosymmetric crystallographic classes (Table 2.2). In these crystal structures, charge centers of the cations and anions do not coincide, the movement of points x, y, z to new points -x, -y, -z causes recognizable differences, which turns the unit cell into an electric dipole[37]. Piezoelectric materials include titanate of barium, lead, and lead zirconate, monoammonium phosphate, and quartz.

Table 2.2 Crystallographic classification according to crystal centrosymmetry and polarity. Groups inside the blue line are piezoelectrics.

Polarity	Symmetry	Crystal system										
		cubic		Hexagonal		Tetragonal		Rhombohedral		Ortho-rhombic	mono-clinic	Triclinic
non-polar (22)	Centro (11)	m3m	m3	6/mmm	6/m	4/mmm	4/m	3/m	3	mmm	2/m	
	Non-centro (21)	432 43m	622 6m2	6	422 42m	4	32			222		
Polar (pyroelectric) (10)			–	6mm	6	**4mm**	**4**	3m	3	mm2	2 m	1

There are some important concepts in piezoelectrics that allows the comprehension of this property[16],[45]:

Piezoelectric voltage constant (g): describes the direct effect (eq. 2.1) by relating the induced electric field (E) to the external stress (X).

$$E = g\,X \qquad \text{(eq. 2.1)}$$

Piezoelectric Strain constant (d): describes the converse effect (eq. 2.2), in which an applied field E produces a proportional strain *s*, the expansion or contraction depend on polarity of E.

$$s = d\,E \qquad \text{(eq. 2.2)}$$

Piezoelectric voltage and strain constants are related by the equation 2.3

$$g = d/\varepsilon_0\varepsilon \qquad \text{(eq. 2.3)}$$

Electromechanical coupling factor (k) is the conversion rate between electrical and mechanical energy and is described by equation 2.4.

$$k^2 = \frac{stored\ mechanical\ energy}{Input\ electrical\ energy} = \frac{stored\ electrical\ energy}{Input\ mechanical\ energy} \qquad \text{(eq. 2.4)}$$

Energy transmission coefficient (λ_{max}): is related to the maximum approach of the input value and is described as follows:

$$\lambda_{max} = \left(\frac{outpu\ mechanical\ energy}{Input\ electrical\ energy}\right)_{max} = \left(\frac{output\ electrical\ energy}{input\ mechanical\ energy}\right)_{max} \qquad \text{(eq. 2.5)}$$

Efficiency (η): is related to the dielectric loss of the material and obtained using equation 2.6.

$$\eta = \frac{Output\ mechanical\ energy}{comsumed\ electrical\ energy} = \frac{output\ electrical\ energy}{consumed\ mechanical\ energy} \qquad \text{(eq. 2.6)}$$

Mechanical quality factor (Q_M): is the magnitude of the resonant strain and characterizes the sharpness of the electromechanical resonance spectrum. It is given by the equation 2.7.

$$Q_M = \frac{\omega_0}{2\Delta\omega} \qquad \text{(eq. 2.7)}$$

Acoustic impedance (Z): is a parameter used to evaluate the acoustic energy transfer between two materials, in general obtained from equation 2.8:

$$Z^2 = \frac{pressure}{volume\ velocity} \qquad \text{(eq. 2.8)}$$

2.2.4 Ferroelectric materials

Ferroelectric materials were discovered by Joseph Valasek around 1920, finding a hysteretic behavior with Rochelle salt, a single crystal material[46]. The term arose in analogy to ferromagnetic materials that present similar characteristics under a magnetic field instead of an electric phenomenon. This is one of the most interesting properties of dielectric solids.[37]

As exposed before, there are 20 non-centrosymmetric systems that possess piezoelectric properties, nevertheless, only the dielectric materials with a reversible spontaneous polarization in the presence of an electric field are called *ferroelectrics*[45]. Therefore, all ferroelectrics are piezoelectric but not in the reverse way[3]. The ferroelectric behavior of crystal is limited by a transition phase point called the Curie temperature T_c, when the temperature exceed this value the material is no longer ferroelectric and exhibits normal dielectric properties[47], in these conditions ferroelectrics present a pyroelectric behavior where the polarization is also affected by the change in temperature.

Ferroelectric materials show a large spectrum of functional properties as high electric polarization, strong piezoelectricity, nonlinear optical activity, great pyroelectricity and nonlinear dielectric behavior. Some promising applications for these materials include high permittivity capacitors, ferroelectric memories, pyroelectric sensors, piezoelectric/electrostrictive transducers, electrooptic devices, and PTC thermistors.[45]

2.3 Barium titanate - $BaTiO_3$

Barium titanate is a typical ceramic ferroelectric that have been widely studied and used for several piezoelectric applications[48]. The main reason for this is that its coupling factors are substantially higher than that of any other lead-free piezoelectric materials (Table 2.3)., except for Rochelle salt (k_p=0.9). In addition, barium titanate have the advantage of being chemically more stable than Rochelle salt, presenting a wider temperature range of operation, and of easy manufacture by several ceramic processing techniques.[45], [48]

Table 2.3 Piezoelectric properties of representative piezoelectric materials. [45]

Parameter	Quartz	$BaTiO_3$	PZT 4	PZT 5H	(Pb,Sm) TiO_3	PVDF-TrFE
d_{33} (pC/N)	2.3	190	289	593	65	33
g_{33} (10^{-3} Vm/N)	57.8	12.6	26.1	19.7	42	380
k_t	0.09	0.38	0.51	0.50	0.50	0.30
k_p		0.33	0.58	0.65	0.03	
$\varepsilon_3^X/\varepsilon_0$	5	1700	1300	3400	175	6
Q_M	$>10^5$		500	65	900	3–10
T_C (°C)		120	328	193	355	

Barium titanate is a member of a large family of compounds with the general formula ABO_3, called perovskites. $BaTiO_3$ assumes different crystallographic structures depending on its temperature (Figure 2.4), below its Curie temperature (T_c=120 °C), the vector of spontaneous polarization points in the [001] direction, corresponding to its tetragonal phase. Below 5 °C, it reorients in the [011] direction (orthorhombic phase). For temperature below -90 °C, the rhombohedral phase is stabilized in the [111] direction. There is also a temperature dependence of the permittivity (ε) that tends to maintain stable values at room temperature (Figure 2.4).[48]

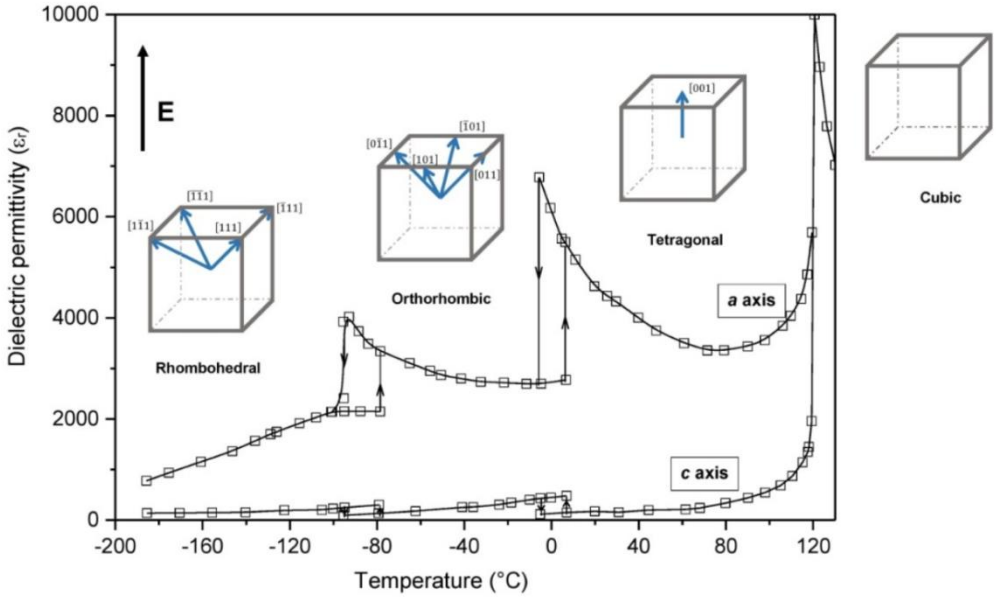

Figure 2.4 Phase diagram of $BaTiO_3$.[16]

Regarding the applications of $BaTiO_3$ at room temperature, it is important to study $BaTiO_3$ in its tetragonal phase (P4mm) which is characterized by a slightly elongated structure of the crystal that yields the spontaneous polarization[45]. The spontaneous polarization is the consequence of the Ba^{2+}, Ti^{4+} and O^{2-} ions location inside the unit cell (Figure 2.5.a). Ba^{2+} ions are located in the unit cell vertices of the cube. When the cubic unit cell is distorted, it occurs a relative shifting of Ti^{4+} and O^{2-} ions from their symmetric positions, which results on appearance of dipolar moments (Figure 2.5.b).

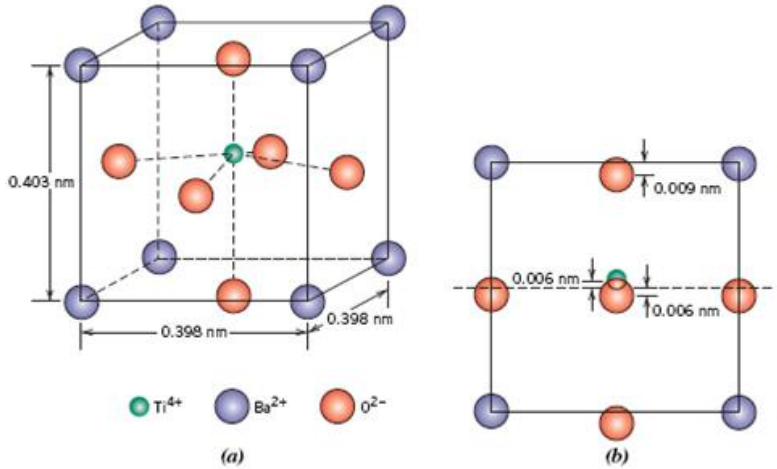

Figure 2.5 Tetragonal unit cell of barium titanate. a) isometric projection b) perpendicular view of one face.

The piezoelectric coefficient matrix for $BaTiO_3$ is represented below, the values will be possible to get after the poling process:

$$\begin{pmatrix} 0 & 0 & 0 & 0 & d_{15} & 0 \\ 0 & 0 & 0 & d_{15} & 0 & 0 \\ d_{31} & d_{31} & d_{33} & 0 & 0 & 0 \end{pmatrix}$$

2.4 Flexible bionanocomposites

The ideal or classical composite is referred to be a continuous amorphous single crystal or polycrystalline matrix, formed by the dispersion of solid particles in a distinct second phase, usually or exclusively of single crystal or polycrystalline character.[49] In particular, piezoelectric layers of moderate thickness (~10-100 μm) are preferable for sensors or actuators.

Piezoelectric films, patches, and adhesives are classified as smart materials due to the presence of a coupling factor (*k*) that is related to the ability of process bending (flexibility) and strain (stretchability) into an electrical signal and vice versa. Prototyping a piezoelectric physical biomedical sensor could be one of the meaningful applications for the biomedical field to approach the advantages of the materials exposed before.[16], [50]
To produce a flexible piezoelectric bionanocomposite, it is necessary to follow some general steps (Figure 2.6).

Figure 2.6 General flowchart for the fabrication of a flexible composite matrix.

The combination of a piezoelectric ceramic with a polymer allows tailoring the piezoelectric properties of the composite.[20] Bionanocomposites can be engineered with desired properties by the variation of ratios or concentration of different types of matrices and reinforcements. These properties strongly depend on the characteristics of raw materials and the manner in which they are connected. There are 10 different ways to describe the orientation of materials in a 3D space: 0–0, 1–0, 2–0, 3–0, 1–1, 2–1, 3–1, 2–2, 3–2, and 3–3 as represented in Figure 2.7. The numbers indicate the continuity of each phase (piezoelectric and polymeric). The 0-3 composites correspond to a polymeric matrix with a homogeneous distribution of piezoelectric particles. The disadvantage of the 0–3 composite geometry is the difficulty in poling as the ceramic phase is not self-connected in the poling direction.[16]

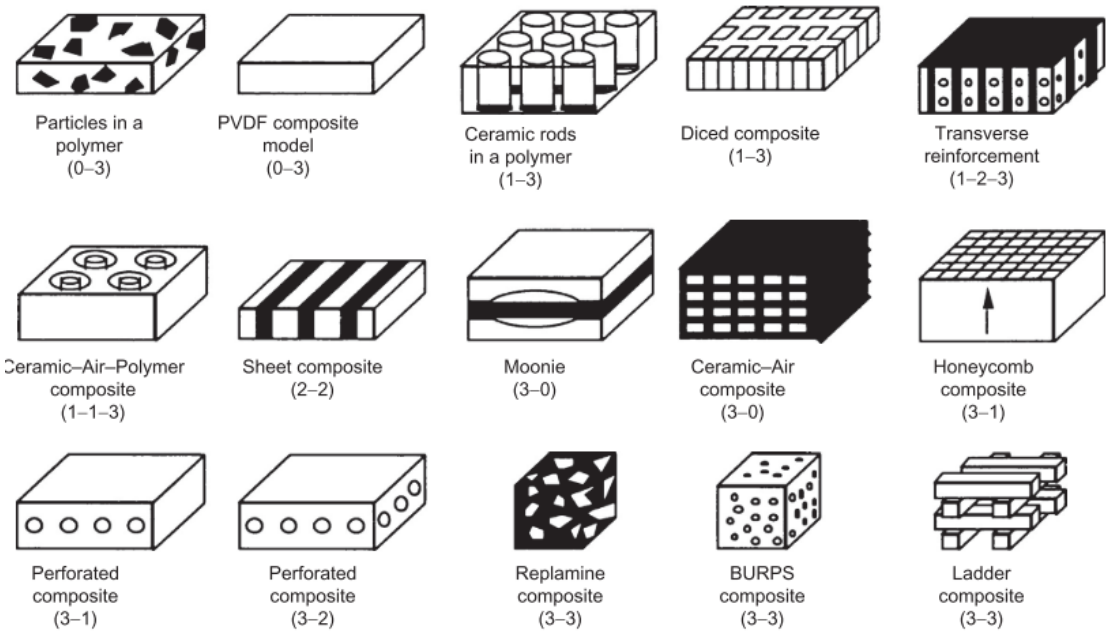

Figure 2.7 Schematic of various piezoelectric composites of different connectivities.[16]

2.4.1 Methods to produce $BaTiO_3$ NPs

Several methods to synthetize $BaTiO_3$ ceramic structures have been developed. Some of the methods are sol-gel method, microwave assisted methods, coprecipitation, microemulsion process, polymeric precursor, and hydrothermal method.[51] The selection of the method depends on the desired application.[29], [52], [53]

Coprecipitation method and solid state reaction are the most used[52]. Nevertheless, the later process requires very high temperatures which increase the energy cost. Due to this reason the hydrothermal synthesis method appears as a viable option to synthetize lead free NPs of barium titanate. Furthermore, it is difficult to obtain $BaTiO_3$ powders with and average grain size smaller than 1 μm using conventional sintering methods, due to the agglomeration processes caused by the high temperatures. Hydrothermal synthesis permits the reduction of the grain size which is important for the piezoelectric response of the product.[51]

2.4.1.1 Hydrothermal synthesis

The growing demand from various industries of smart materials with more sophisticated features requires the development of synthesis methodologies very well-defined and

capable of controlling specific features, such as size, shape (morphology), chemical composition, degree of defects, and surface functionalization. Despite of yielding superior products or devices with better functionalities, the advanced synthetic methods should also be inexpensive and environmentally friendly. The low-temperature hydrothermal synthesis meets all of the above requirements[51]. Moreover, it is very well suited to produce both smart ceramics starting materials, such as powders or fibers, and already shaped products, such as bulk ceramic pieces, films or coatings, and single crystals. Consequently, a large family of smart ceramics has emerged. As these materials can be prepared under very mild hydrothermal conditions (T < 200 °C and autogeneous pressure, P < 1.5 MPa), they have generated lots of commercial interest [54]–[56].

Hydrothermal synthesis is a process that utilizes single or heterogeneous phase reactions in aqueous media at specific temperature (T > 25 °C) and pressure (P > 100 kPa) to crystallize ceramic materials directly from solution. The reagents in the hydrothermal synthesis are usually in the form of solutions, gels, or suspensions. Syntheses are usually conducted at autogeneous pressure, which corresponds to the saturated vapor pressure of the solution at the specified temperature and composition of the hydrothermal solution.[51]

One of the main advantages of the hydrothermal method consists in the capability to produce high purity and crystalline powders. As precursors are not in contact with any other material, neither the oxygen or carbon dioxide, the resulting materials are free from $BaCO_3$ (typical formed during coprecipitation). Furthermore, powders do not need milling avoiding their contamination. The obtained particles are also homogeneous in their size which could reach values <1 μm.[55]

2.4.2 Solvent casting method to produce thick films

The solvent casting method is the predominant process to make films of chitosan for macroscale applications. It was invented in 1999 by Mikos *et al.*[57] to overcome the drawbacks associated with the fiber bonding technique and remains as an interesting technique for the biomedical sector. Consist of coating a surface with the desired polymer solution and by evaporating the solvent, it is produced a solid film with a thickness dependent on the dispersed solution concentration. To coat the surface a pipette or a spin coater can be used. It is possible to elevate the temperature with the objective of speed up the solvent evaporation. For chitosan films, the temperature must be around 35 °C.[58] In

comparison to other methods, the solvent casting technique leads to more ductile structures which can be useful for the desired film bending properties.[57]

2.4.3 Electroding and poling process

Spontaneous polarization is not enough to obtain a macroscale response of a ferroelectric because of the randomly distribution of the Weiss domains (groups with the same dipole orientation) throughout the sample. Hence the material needs to pass through a poling process where those dipoles oriented in the opposite direction of the desired one, reverse their orientation by the application of a strong electric field [59](Figure 2.8).

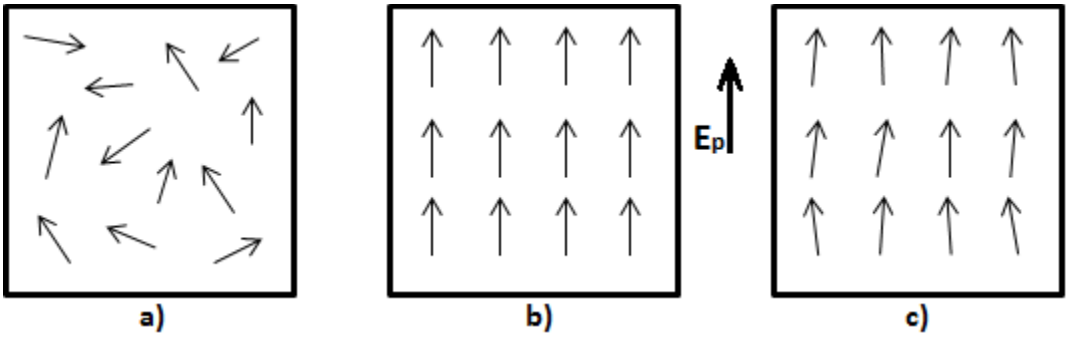

Figure 2.8 Dipoles orientation in a ferroelectric material: a) random orientation of dipoles in absence of an electric field; b) Reorientation of dipoles during a poling process; and c) dipoles arrangement after stop the application of the electric field.

Typically, poling is performed under high electric field with temperature to facilitate domain alignment. Furthermore, if the applied electric field is small, it will not be able to reorganize the dipoles and the material will have a normal dielectric behavior. There is an important phenomenon of dielectrics, called electric polarization, that could be expressed quantitatively as the sum of the electric dipoles per unit volume$[C/m^2]$. The electric polarization results from the reorientation of electrons, ions and dipoles.[60] The degree of contribution of each depends on the frequency of the applied field. Electric and ionic contributions respond to frequencies up to THz-PHz and GHz-THz, respectively. The permanent dipole reorientation response happens only up to frequencies of MHz-GHz. This explains the decreasing behavior of permittivity with the increasing of frequency in the ferroelectric materials.[45]

The polarization process is described in Figure 2.9. The polarization increases linearly with the applied field from 0 to A, as the electric field is not larger enough to promote the orientation of the domains. In the portion A to B, the domains start to orient toward the direction of the field and the polarization increase in a nonlinear way with the increasing of the electric field. As the applied field increases, most of the domains will be aligned to the same direction of the poling field producing a saturation state of the polarization (portion B to C). If the electric field is decreased, the polarization will decrease following the C-B-D path. When the field is equal to 0 the section 0 to D define the remnant polarization. The path 0 to E is the extrapolation of the B to C section, corresponding to the spontaneous polarization. The portion 0 to R is related to the coercive field, which is the necessary field to bring the polarization to zero. When the field in the opposite direction decreases to zero (G to H path) the polarization is reversed and indicates that domains have already been formed before poling and the motion of the domain walls results in the change of direction of the polarization.[16], [37] The hysteresis loop is generally measured with an alternating current (AC) at low frequencies (60 Hz or lower) to avoid heating the specimen.

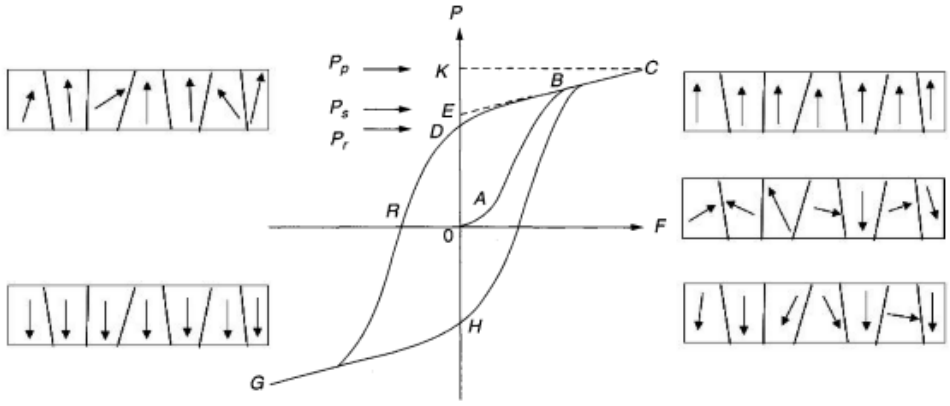

Figure 2.9 Schematic diagram of a typical ferroelectric hysteresis loop with indication of the dipoles arrangements. [37]

2.4.4 Current development of flexible piezoelectric bionanocomposites for biomedical applications

The interest in piezoelectric properties of lead-free bionanocomposites have been an important field in the reasearch of flexible materials for biomedical aplications. In relation to the biopolymer, the known properties of chitosan as film former and filler immobilizer

have been of wide interest for researchers. Furthermore, its cationic nature led to the possibility of its application to biomedical sensors. In collagen-chitosan films the presence of the polysacharide increased the piezolectricty of the composite from 0.096 pC/N (d_{14} for collagen) to 0.212 pC/N and suggested the possibility of using this type of films for electronic devices based in mechanical waves [61]. Later, the dielectric properties of collagen-chitosan films prepared by solvent casting method were confirmed by its enhacement due to the presence of chitosan. This films have an increasing in dielectric permitivity from 2.60 to 3.94 at 1 MHz [62].

Two different works reported the development of cellulose-chitosan films produced by spin coating method for sensor/actuator application. By measuring dielectric properties with LCR meter (Inductance, capacitance and resistance measurements), they found an improvement of relative permitivity caused by the adition of chitosan and higher values were determined for pure chitosan membranes. [63],[64] The electromechanical performance was characterized by the implemetation of a designed setup were the bending response at various frequences and voltages (function generator) was obtained. The maximum bending displacement output was of 4.1 mm achieved at 6 V and 4 Hz at room humidity. These type of material could be useful as smart materials for sensor and actuator mainly in biomedical field.

In the last decade, green piezoelectric materials based on cellulose and chitosan were development. Cellulose nanofibril films were produced using the solvent casting method for sensor applications. The membranes have around 45 μm thick, dielectric constant and dielectric losses of ε_r=3.48 and Tanδ=0.011, respectively, and a d_{33}=4.7 pC/N to d_{33}=6.4 pC/N [65]. The setup for these measurements used a mini-shaker to generate a dynamic excitation force and a sinusoidal input for the shaker provided with a function generator. Hänninen A. *et al*[66] fabricated four biocomposite films with cellulose nanocrystals and nanofibers with chitosan. The mean thickness of the membranes was around 20 μm and 40 μm and the membranes revealed piezoelectric behavior by using the same setup described previously.

The piezoelectric properties of chitosan for applications in vibration sensors was related to the presence of a second harmonic generation response related to the non-centrosymmetric

configuration of the polymer and, therefore, a piezoelectric property of the material [24]. This study also used barium titanate [28] and zinc oxide [67] as fillers in chitosan based films, the measured d_{33} coefficient was obtained by the analysis of the response to a 80 Hz wave in a shaker at 1 g level . Their results suggest an electret [1] behavior of the bionanocomposite produced.

In others research, barium titanate has been used as filler in other polymers for sensor and generator applications. For instance, films of $BaTiO_3$ NPs immersed into polyvinylidene fluoride PVDF prepared by solvent casting method were used to implement ITO/PET as electrodes and measured d_{33} response, obtaining the voltage generated in open circuit from the samples at mechanical excitation. [68] Other work reported results about $BaTiO_3$ (nanoparticles from 20 to 70 nm) immersed at different concentrations into TiO_2 and PMMA [69]. The films revealed dielectric properties and the relative permittivity decreased with the increase of frequency.

In the majority of cases, the reported dielectric constant is related to a variation of frequency, in piezoelectric composites (polymer based), the quantification of this value is given by the analysis of the electric charge density derived from an excitation at different frequencies. The reported response is divided in very low frequencies response (quasi-static piezoelectric coefficient) and dynamic piezoelectric coefficient obtained by the measurement of the charge density per unit of stress to an applied range on frequencies. [70]

[1] Electret: Term coined by Oliver Heaviside in 1885, describes the effect of quasi-permanent charge or dipole polarization. This phenomenon is usually present in voided charged polymers. After the poling process, the charges embedded into the polymer are charged and form dipoles, these dipoles respond to external mechanical forces or fields, similar to piezoelectric materials. In this type of material the piezoelectric effect is not due to a non-centrosymmetric center in a crystalline structure but because of the deformation of the free space charges in the material[70].

Chapter 3 Experimental Section

3.1 $BaTiO_3$ particles production

Hydrothermal method was used to form $BaTiO_3$ nanoparticles following the procedure proposed by Lin *et al.*[29]. Two types of $BaCl_2$ (hydrated and non-hydrated) precursor were considered for the experiments. The general procedure was the following: 0.25 g of TiO_2 (P25, Aldrich) and 0.76 g of $BaCl_2 \cdot 2H_2O$ (99.9%, Merck) or 0.65g of $BaCl_2$ (99.9%, Aldrich) were added to 20 mL of 10 M aqueous solution of NaOH previously prepared. The mixture was then transferred into a 25 mL Teflon-lined stainless-steel autoclave and left at 200 ºC for variable time, as shown in Table 3.1.

After taking out the samples from the oven, they were washed/centrifuged several times until neutral pH, using a centrifuge at 6000 rpm speed. Powders were dried at 60 °C and reserved for further use. Samples were named H_*y*h or nH-*y*h in which H or nH stands for hydrated or non-hydrated barium chloride, respectively, the *y* represents the number of hours of synthesis.

Table 3.1 Temperature and reaction time conditions used for the syntheses of $BaTiO_3$ particles.

Barium precursor	Sample designation	Time (h)
H	H_2h	2
	H_6h	6
	H_24h	24
	H_48h	48
	H_72h	72
nH	nH_24h	24
	nH_72h	72

3.2 Films preparation

Considering the type of matrix and reinforcement, the fabricated films are classified as polymer particulate matrix composites or 0-3 biocomposites.[20] A chitosan solution 1.5 % (w/v) was prepared by dissolving the chitosan (medium molecular weight, 85% of deacetylation, Aldrich) in 5% (v/v) aqueous acetic acid (Aldrich, ≥ 99.7%) solution with stirring for 20 h at room temperature. Glycerol (Fisher Chemicals, 98%) in a concentration

of 0.5% (w/w) was added to the resulting solution and the mixture was left at 50 ºC, with stirring, for 10 min to promote better homogenization. After stirring for more 30 min at room temperature, the solution was filtered into a Büchner flask with a nylon mesh using vacuum and degassed to remove bubbles. The obtained solution (31 g) was distributed into plexiglass plates of 144 cm^2 and 3 mm deep. The plates were placed in the oven for 24 h at 35 ºC in order to allow film formation by solvent casting. After, removing from the plates, the films were stored for 5 days in a camera with relative humidity of 52% RH (saturated magnesium nitrate solution at room temperature) to equilibrate. The film obtained was prepared to act as control or blank and named as C (Table 3.2).

For the Chitosan-$BaTiO_3$ films the same procedure was followed but adding the selected quantity of synthetized $BaTiO_3$ particles at the same time of chitosan powder. The quantity of $BaTiO_3$ was calculated based on chitosan quantity and the films were designed as *x*_ Ratio chitosan:$BaTiO_3$, H for hydrated barium chloride.

Table 3.2 Nomenclature of the films prepared using the synthetized particles and increasing the quantity of $BaTiO_3$ for each case.

Film designation	$BaTiO_3$ particles	Ratio Chitosan:$BaTiO_3$ (m:m)
C	none	0
H_1:0.4	H_24h	1:0.4
H_1:0.5		1:0.5
H_1:0.6		1:0.6
H_1:0.8		1:0.8
H_1:1.5		1:1.5
H_1:2.0		1:2.0

3.3 Structural and morphological characterization

Different characterization methods were used to find the properties and behavior of particles and films.

3.3.1 X-ray diffraction (XRD)

The X-ray technique is versatile and non-destructive and was used for the qualitative and quantitative analysis of the $BaTiO_3$ crystallographic phases present in the samples. The XRD was performed using Philips X-pert MDP equipment with Cu-Kα X-radiation and λ=1.5406 Å. The sweeping angles used for identification of the crystalline phases in $BaTiO_3$ particles were from 20° to 80° with a step of 0.02° at room temperature. For phase identification through the X-ray diffraction peaks, an integrated database of Powder Diffraction Files (PDF) from the International Centre of Data Diffraction (ICDD) was used. The Scherrer equation (eq. 3.1) was used to calculate the crystallite size.

$$\tau = \frac{K\lambda}{\beta \cos \theta} \qquad (eq. 3.1)$$

Where, τ is the mean size of the ordered domains, K is the shape factor (typically 0.9), λ is the X-Ray wavelength, β is the line broadening at half the maximum intensity (FWHM) and θ is the Bragg angle.

3.3.2 Scanning Electron Microscopy (SEM)

Scanning Electron Microscopy was used to study the microstructure of $BaTiO_3$ particles as well as their dispersion on the biopolymer matrix. The Hitachi® model SU-70 was used for SEM. This microscope can achieve magnifications from 30 to 800000 times with acceleration voltage in range of 0.1 to 30 kV. The images were taken with magnifications from 3000 to 50000 times at 15 kV. To prepare the samples, the obtained powders were put in carbon tape over platinum substrate. The films were stacked onto a typical SEM sample-holder with carbon tape. All samples were coated with carbon for the observation.

The obtained images also served to estimate the particle size assisted by the software ImageJ version 1.5[71]. Around 100 particles from the images were measured to obtain the average particle size.

3.3.3 Raman spectroscopy

Raman spectroscopy is known to be more sensitive to shorter range order than XRD and constitutes a powerful method to probe the microstructure of nanoparticles. Raman spectroscopy was used to confirm the tetragonal phase of $BaTiO_3$ as this phase is non-

centrosymmetric presenting a characteristic Raman spectrum. The Raman spectra were obtained using the FT Raman spectrophotometer RFS 100/S (Bruker), with a 4 cm^{-1} resolution a YAG-Nd laser (1064 nm) as the excitation source and a He-Ne laser as the alignment source. Particles and films were scanned 500 and 700 times, respectively.

3.3.4 Fourier Transform Infrared spectroscopy (FT-IR)

The FTIR analysis of the films was performed in a Golden Gate single reflection diamond ATR reflection system (Perkin Elmer Spectrum BX). The spectra were acquired at the absorbance mode between 4000 and 400 cm^{-1} (mid infrared region) with a resolution of 4 cm^{-1} and 32 scans. Five replicates were collected for each sample.

3.3.5 Contact angle

The contact angle was measured using the system OCA 20, Dataphysics. The films were cut in six strips of 1x6 cm and analysis were performed, three on the top side and three on the bottom one. The syringe of the system was filled with ultra-pure water and the system was programed to dispense drops of 3 µL automatically. For each measurement the system recorded the result using an integrated camera and the data was processed using the SCA20_M4, Dataphysics software. There were dispensed nine drops for each sample.

3.3.6 Mechanical Properties

The mechanical properties of the films were evaluated through tension until rupture tests following ASTM D 882 and 883 practices. The texturometer used was a TA-HDi, Stable Micro Systems. The *Young modulus* (Y) (eq. 3.2) corresponds to a value used to express film elasticity and it is the slope of stress-strain curves (figure 3.1) in its linear section. It is achieved by dividing the tensile stress (St) by the extension strain (S). The *tensile strength* (eq. 3.3) allows to know the force in MPa needed to break the films. The *elongation at break percentage* (eq. 3.4) shows the increasing in the length of the film until breaking in response to the application of contrary forces.

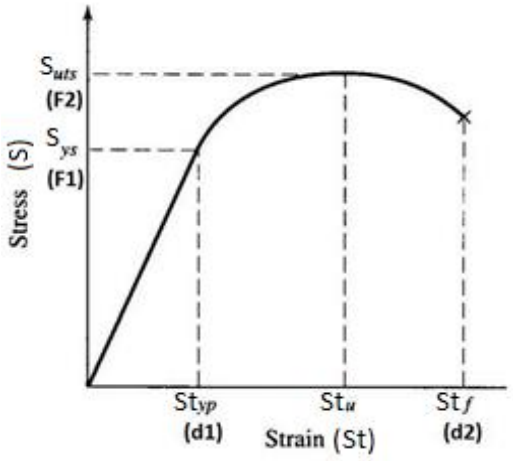

Figure 3.1 Strain as a function of the stress curve.

$$Y = \frac{St}{S} = \frac{F_1 * L_0}{A_{crossection} * d_1} \qquad (eq\ 3.2)$$

$$tensile\ strength = \frac{F_2}{A_{crossection}} \qquad (eq\ 3.3)$$

$$\%\ elongation = \frac{d_2}{L_o} * 100 \qquad (eq\ 3.4)$$

The samples were prepared by cutting 5 strips (of each film) of 1 x 9 cm marking 2 cm from the ends to attach the equipment grips, leaving 5 cm^2 as exposed area (L_o). The mean films thickness was calculated by measure five points of each strip immediately before the tests with a digital micrometer (*Digimatic Micrometer MDE-25PJ, Mitutoyo*), to calculate cross sectional area ($A_{crossection}$). The means were calculated and used in the determination of mechanical properties. The films were tested in a room with controlled temperature and humidity of 27 ºC and 57±5%, respectively. The tests used a rate of 0.5 mm/s extensional deformation until sample rupture.

3.3.7 Humidity

To determinate the films humidity it is necessary to dry the films at 105 °C until get a constant weight. Three samples of each film were cut in squares of 4 cm^2 and were weighted. Afterwards, the films were left in an oven at 105 ºC during 20-24 h. The dried films were placed in a desiccator for 30 min to cool down and then weighted again. The film humidity is calculated using the following equation:

$$\%\ humidity = \left(\frac{m_{film\ i} - m_{film\ f}}{m_{film\ i}}\right) \times 100$$

Where $m_{film\ i}$ is the mass of the initial film and $m_{film\ f}$ is the mass of film after drying at 105 °C. The films humidity determination is made in triplicate.

3.3.8 Solubility

The solubility of the films was determined by the difference in mass of the samples before and after being immersed in water for a specific period of time. Three squares of 4 cm^2 from each film were weighted and left in 30 mL of distilled water at room temperature for seven days. Then, the films were taken out from the water and put in the oven at 105 ºC for 24 h. The samples were placed in a desiccator for 30 min to cool down and then were weighed again. The solubility of the films is determined using the following equations:

$$\% \, Solubility = \left(\frac{m_{\,film\,i\,dried} - m_{film\,f\,dried}}{m_{\,film\,i\,dried}} \right) \times 100$$

Where $m_{\,film\,i\,dried}$ is the initial mass of the dried film and $m_{film\,f\,dried}$ is the mass of film after it was submerged in the matrix and dried.

3.3.9 Statistical analyses

The obtained results from solubility, humidity, contact angle and tensile mechanical properties where analyzed by F-tests and T-student tests in Microsoft excel 2010, to find the relation between the samples with a significance level of 5%. The samples were considered significantly different if the level of significance $p < 0.05$.

3.3.10 Electrical measurements

The films were cut in squares of 1 cm^2 to determine their electrical characteristics. The samples were coated with gold electrodes (r=3 mm) on both sides using an ion evaporator (*Polaron SEM Coating Unit E5000*). Electrical measurements were made using the LCR meter (*Hewlett Packard 4284 A*) and measures were taken for a frequency rank between 100 Hz and 1 MHz and voltage of 1 V. Values of dielectric permittivity, dielectric loss factor (Tan δ), conductivity, and resistivity were obtained.

To determine the piezoelectric behavior of the films, the poling process was done using the corona tip discharge. Samples were placed into a Faraday cage at 80 °C and then consecutive discharges were made during 30 min at 10 kV using a high voltage font (*EQ Series 1200 Watt Regulated High Voltage DC Power Supplies*). The d_{33} and couple factor (*k*) were measured using a *YE2730 d_{33} meter* equipment that applies a specific pressure of 0.25 N in the normal direction of the material. This force was applied cyclically to a square

wave signal of 110 Hz and measured the voltage. The d_{33} value is giving in pC/N. The calibration of the equipment was made by measuring a pattern and adjusting the zero before each test.

The hysteresis loops for were obtained for 1:2 samples using a hysteresis tester that includes an amplifier (TREK model 610E or 609E-6). The measurement procedure involved the application of a triangular voltage waveform.

Local ferroelectric/piezoelectric properties were investigated with PFM and images were obtained by applying ac voltage (variable value peak-to-peak) with frequency of 50 kHz (out of plane) and 5 kHz (in plane) using a commercial AFM (Ntegra Prima, NT-MDT) with home-made Piezoresponse Force Microscopy (PFM) setup. A conductive tip is used to apply an electrical bias and to detect the local electromechanical response of the sample. Analyses were supported by the scanning probe microscopy software WSxM 5.0 develop 0.1 (Copyrigth © January 2018). Schematic of the Piezoresponse Force Microscopy (PFM) arrangement is presented in Figure 3.2. Voltage is applied between the conducting tip and the sample and mechanical displacement is measured via conventional contact Atomic Force Microscopy (AFM) method using additional lock-in amplifier.

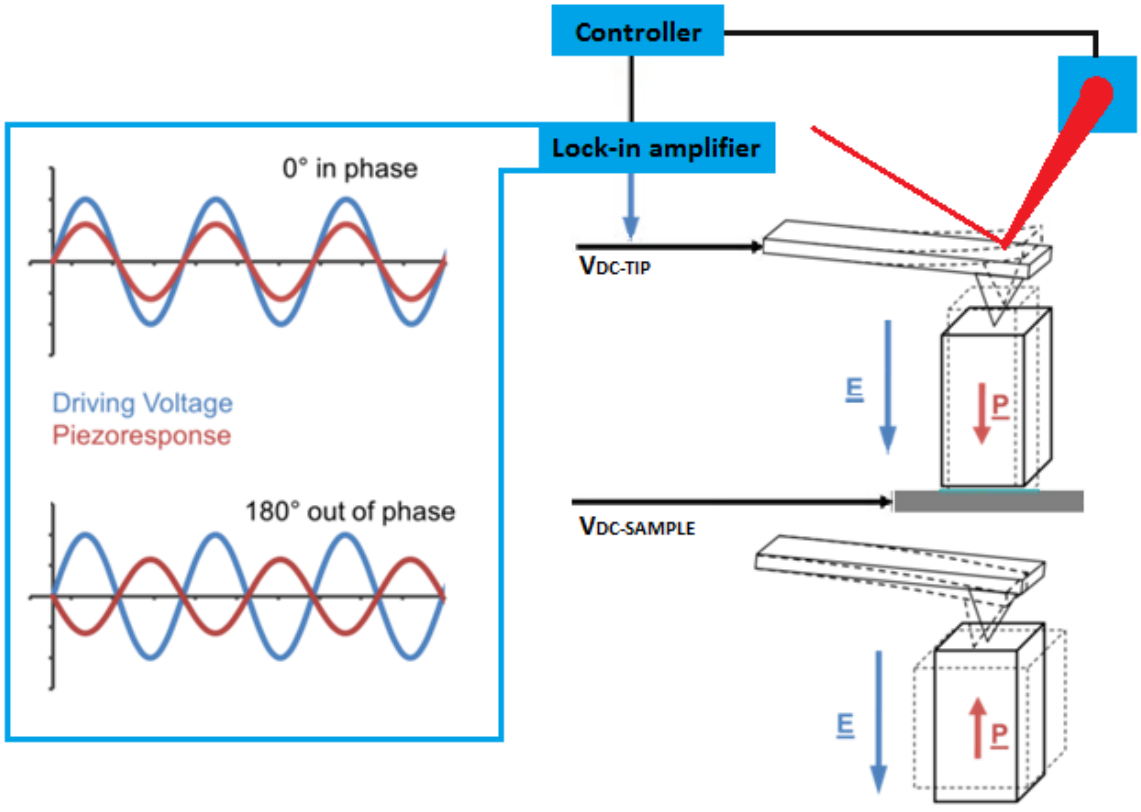

Figure 3.2 Scheme of the piezoresponse force microscopy arrangement.

Chapter 4 Synthesis and characterization of $BaTiO_3$ particles

4.1 Characterization of the samples

Various experiments were done to obtain $BaTiO_3$ in its tetragonal crystallographic phase which has ferroelectric properties at ambient temperature. All the syntheses were performed at a temperature of 200 °C, which is a reasonable value to synthetize $BaTiO_3$ in a well-defined tetragonal phase[53]. Dihydrated barium chloride and P25 titanium precursors were applied in syntheses using variable reaction times from 2 to 72 h.

Figure 4.1 shows the SEM microimages obtained for each reaction. Particles size increases and becomes more heterogeneous over the time of reaction. After two hours of reaction, the particles are almost spherical with a mean size of 46 nm. A remarkable change in the particles shape is observed after 24 h (Figure 4.1.c), since they show a defined cubic form. This behavior remains until 72 h of reaction (Figure 4.1.c-e), when particles reach a mean size of 583 nm. Figure 4.1f shows a plot of the particles size mean versus the reaction time. The slope shows that the growth rate was higher from 6 to 24 h of reaction than from 24 till 72 h. The most significant increase of the particles size happens in the first 24 h of reaction.

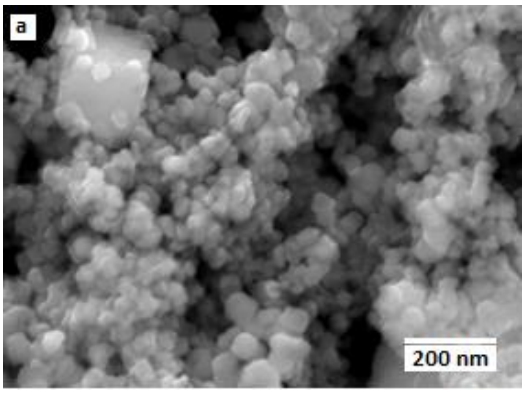

H_2h: S_{SEM}=46±30 nm

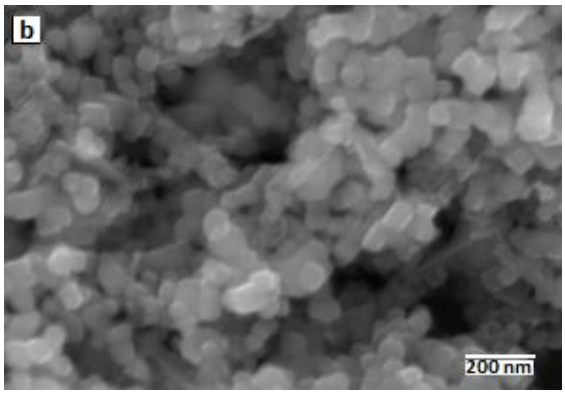

H_6h: S_{SEM}=74±17 nm

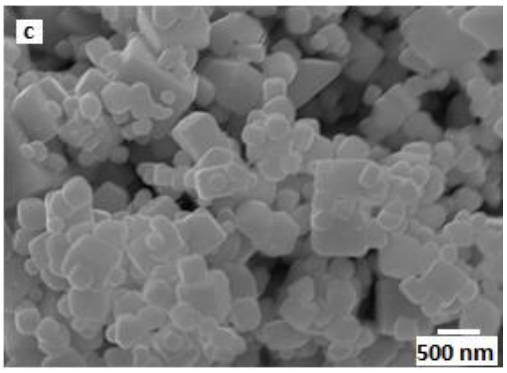

H_24h: S_{SEM}=306±100 nm

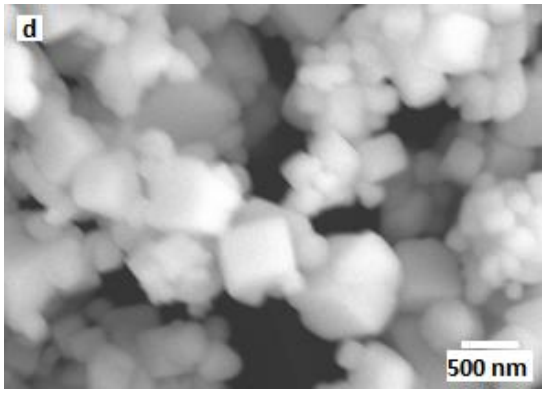

H_48h: S_{SEM}=427±118 nm

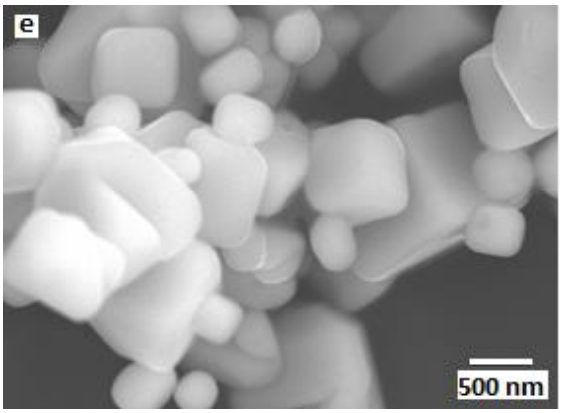

H_72h: S_{SEM}=583±192 nm

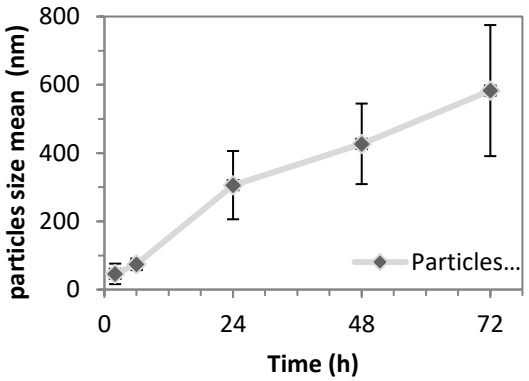

f) Time/ particles size mean plot

Figure 4.1 SEM micrographs of samples: a) H_2h; b) H_6h; c) H_24h; d) H_48h; e) H_72h indicating the average size of about 100 particles measured with imageJ. f) shows a plot of the particles size mean as a function of the reaction time.

The presence of tetragonal phase was studied using XRD and Raman techniques. Figure 4.2 shows the XRD patterns for each sample of $BaTiO_3$ compared with peaks from JCPDF cards for cubic and tetragonal crystallographic phases. The results show that all samples present the representative peaks of $BaTiO_3$. Nevertheless, H_2h and H_6h samples present more noisy patterns what should be related with a pseudo-crystallization of the particles and/or small size of the particles.[55]

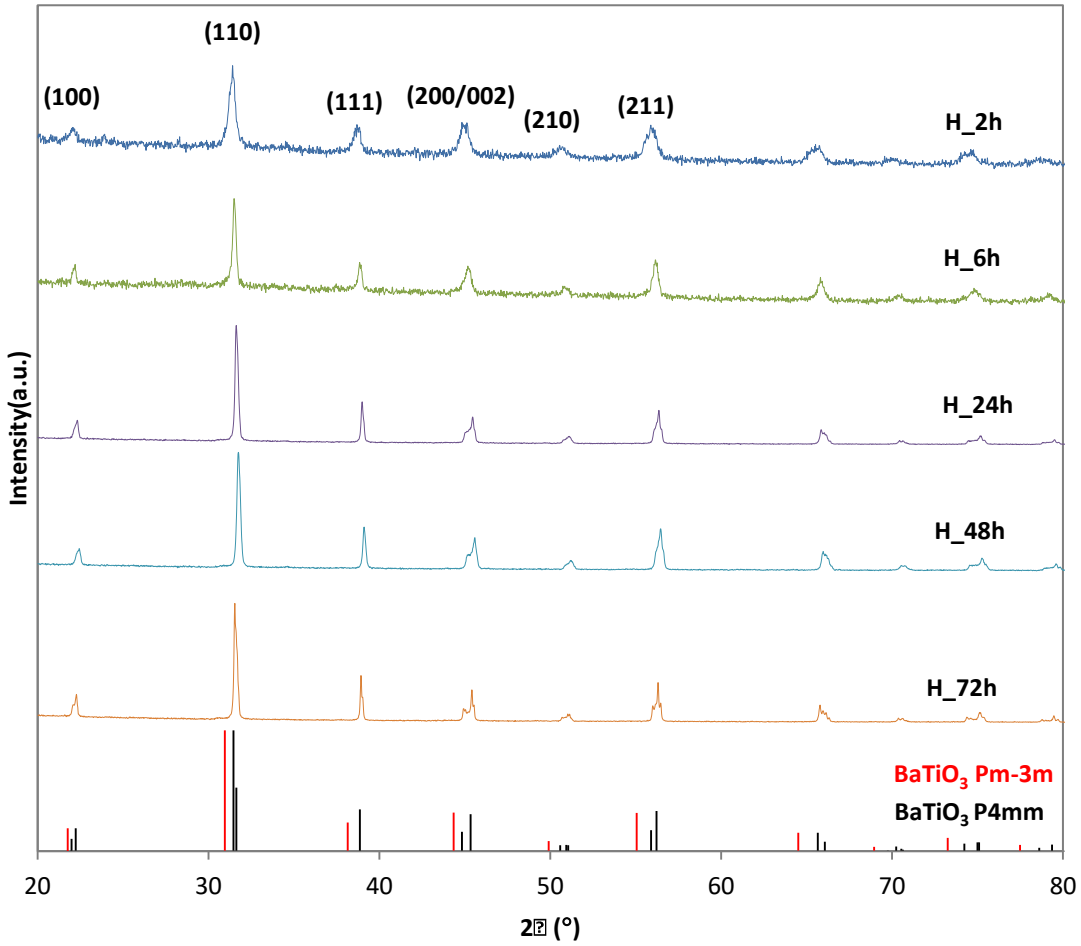

Figure 4.2 XRD analyses of H_2h, H_6h, H_24h, H_48h, H_72h $BaTiO_3$ NPs against tetragonal $BaTiO_3$ reference card (nr. 04-016-2040) and cubic $BaTiO_3$ reference card (nr. 04-006-2614) .

The splitting of some of the peaks of the XRD pattern is related with the crystallization of the tetragonal phase[72]. Although, the splitting of the peaks around 44-46° 2θ is better defined after 72 h of reaction (Figure 4.3), the XRD pattern after 24 h of reaction, already shows this splitting. The 24 h time of reaction was the selected time for the synthesis of particles using the barium chloride dehydrated precursor. This time of synthesis ensures a better homogeneity of the particles size while allows a more sustainable synthesis in terms of duration of reaction.

Crystallite size was calculated using the Scherrer equation (eq. 3.1); the 111 peak was selected because it is a single peak both in cubic or tetragonal crystallographic phases, which permits to estimate the FWHM value with more precision. Table 4.1 shows the grain size calculated by using the ImageJ software and the crystallite size calculated from the XRD patterns. It is worth to confirm that the measured crystallite size is always lower than estimated mean particle size.

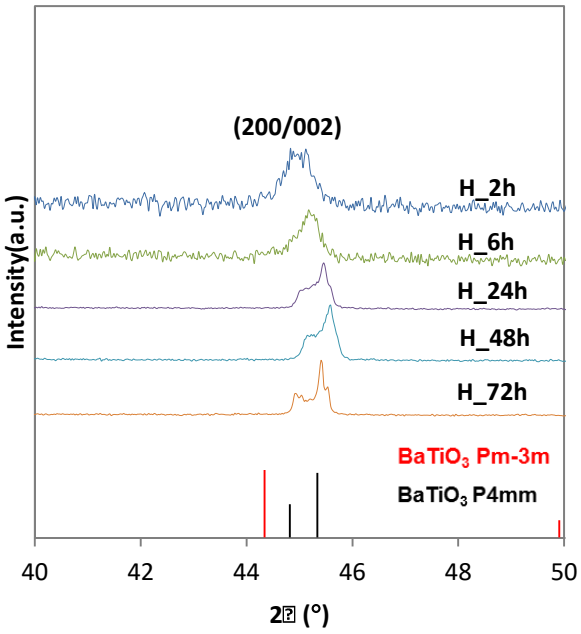

Figure 4.3. Magnification of the 200/202 peaks to observe the splitting that proves the presence of tetragonal and cubic $BaTiO_3$.

Table 4.1. Results for $BaTiO_3$ crystallites and crystal sizes (*average value resulting from the measurement of ca. 100 particles using ImageJ; ** calculated using Scherrer equation).

Sample	D_{SEM}* (nm)	D_{XRD}** (nm)
H_2h	46	19
H_6h	74	52
H_24h	306	114
H_48h	427	250
H_72h	583	480

Raman spectroscopy was used to confirm the presence of tetragonal phase in $BaTiO_3$ particles. Figure 4.4 shows the obtained spectra for all samples correlated with the expected Raman modes. Besides of confirming the presence of tetragonal phase in every sample, the designated bands (183, 307, 513, 712) cm^{-1} reveal the definition of tetragonal structure of the molecules. For instance, peaks around 513 cm^{-1} and 185 cm^{-1} belong to the fundamental TO (transverse component) modes of A1 symmetry group, and the broad band around 513 cm^{-1} is associated to its longitudinal mode (LO). The E (TO) component around 307 cm^{-1} is related to the asymmetry of TiO_6 octahedra of $BaTiO_3$ on a local scale. Sharpness in this peak shows the dominance of tetragonal phase in the sample. Therefore, 24 h and 72h reaction times were selected for the studies with the non-hydrated precursor.

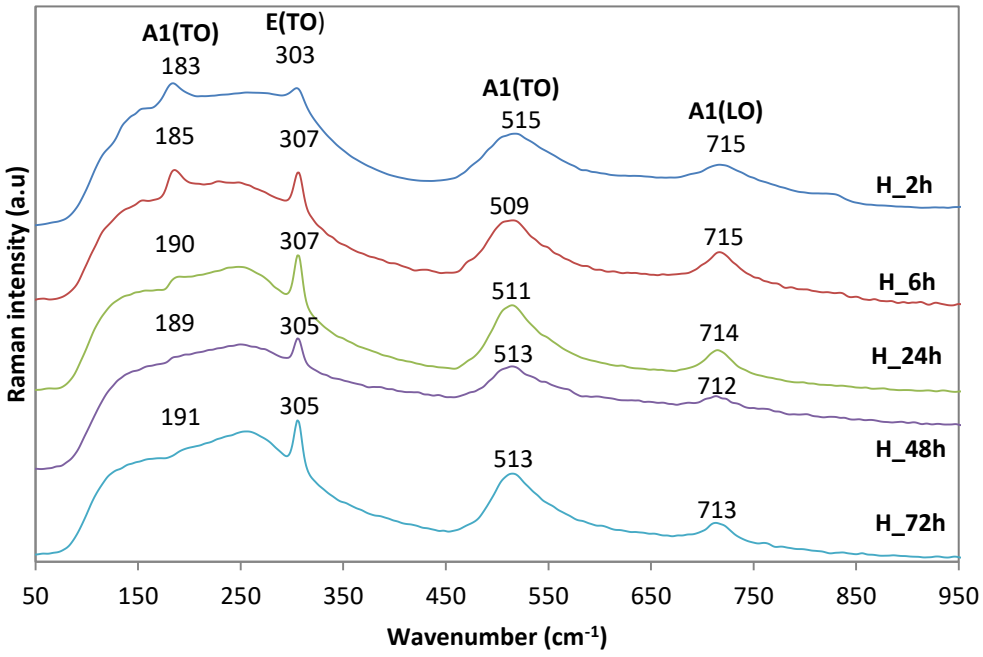

Figure 4.4 Raman spectra of samples H_2h, H_6h, H_24h, H_48h, and H_72h.

Figure 4.5 shows the SEM micrograph images of the samples prepared with the non-hydrated barium chloride for 24 and 72 h of reaction time. The shapes of the obtained particles were very similar to the ones synthetized with hydrated barium chloride (cubic),

but approximately 100 nm bigger and more homogeneous. Several authors reported that the precursor may have a strong influence on the size and morphology of $BaTiO_3$[30], [52], [55]. For example, Zong-Hong L. *et al*[29]. used a similar protocol and obtained particles with nanotubes morphology. In our case, the use of non-hydrated barium chloride did not lead to the anisotropic shape. The use of hydrated or non-hydrated precursor did not resulted in very significant differences on the particles morphology; both particles show cubic like shape. Nevertheless, it is noticed some discrepancies between the particle sizes which may be an indicative of the different reactivity of the non-hydrated precursor.

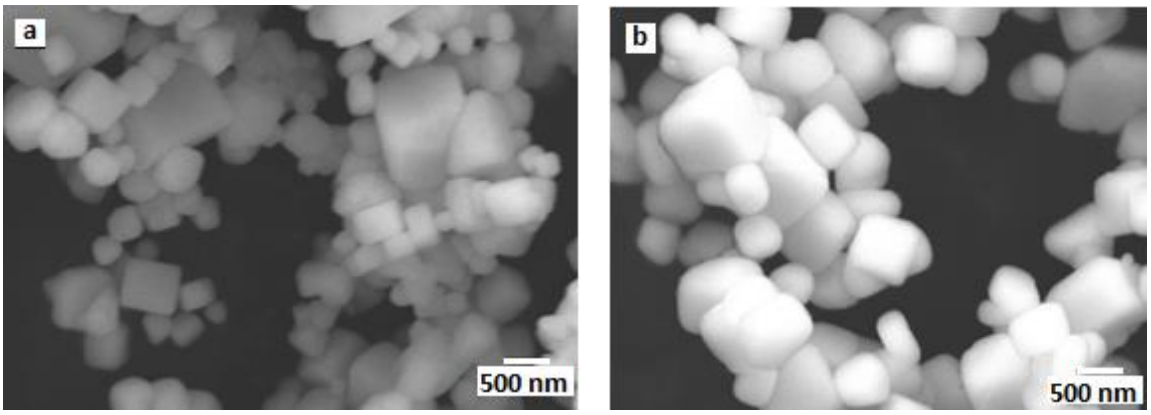

nH_24h: SSEM=478±90 nm

nH_72h: SSEM=625±60 nm

Figure 4.5 SEM micrograph of samples: a) nH_24h; b) nH_72h indicating the average size of about 100 particles measured with imageJ

XRD and Raman techniques were also used to characterize the obtained particles. Figure 4.6 shows the comparison between XRD spectra of the particles of H and nH samples for 24 h and 72 h of synthesis and Figure 4.7 shows Raman spectra. The comparison between the samples shows the presence of the respective bands for $BaTiO_3$ in each sample, confirming the presence of tetragonal phase.

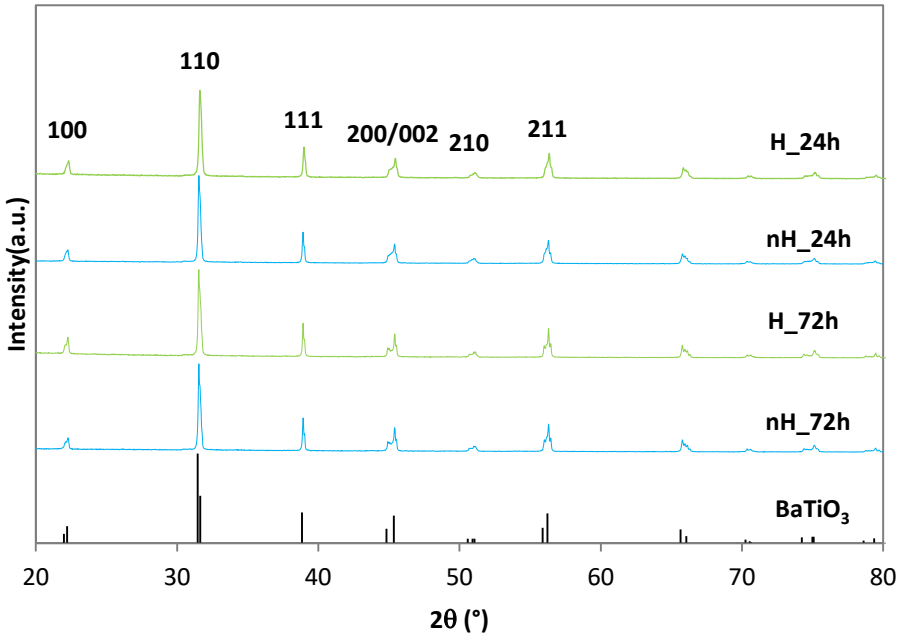

Figure 4.6 Comparison of XRD diffractograms of H_24h, nH_24h and H_72h, and nH_72h samples.

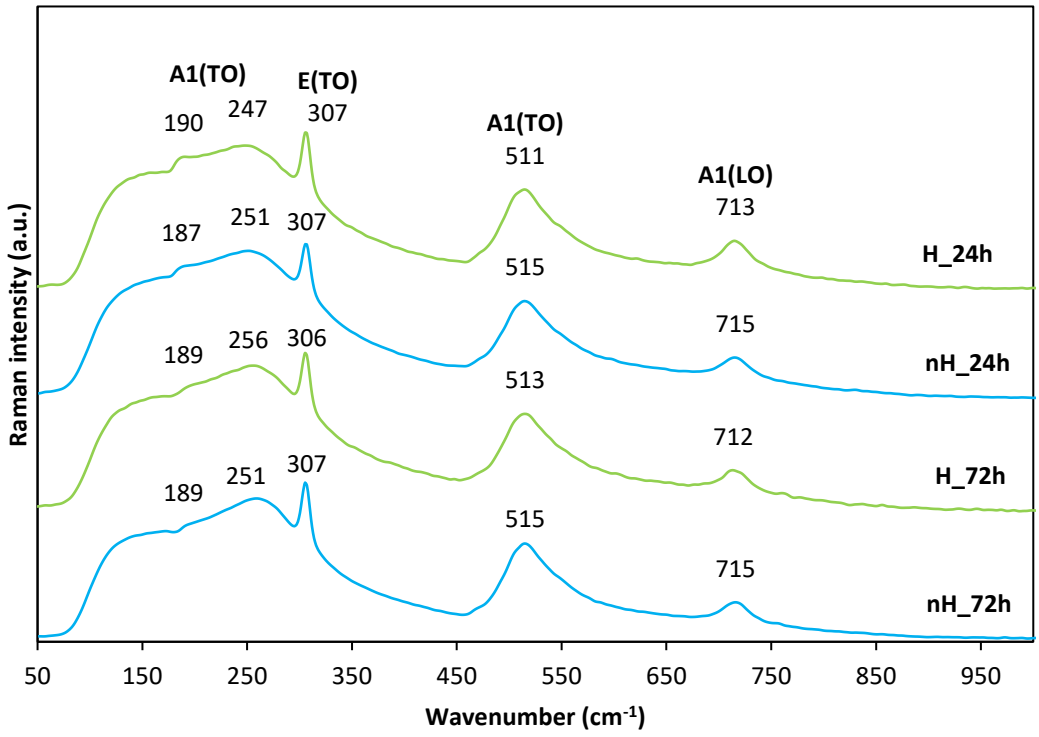

Figure 4.7 Comparison of Raman spectra of H_24h, nH_24h, H_72h, and nH_72h samples.

As the obtained particles were similar, more particles using H_ and nH_72h 24h conditions were synthetized to be used in the fabrication of the films, confirming if there is any difference by using particles with different times of reaction. Different batches were mixed for each type of particles used (H_24h and nH_72), dried at 60 °C and kept under dried conditions up to the film fabrication. These bulk samples, resulting of the mixture of various batches, were characterized by SEM (Figure 4.8), XRD (Figure 4.9) and Raman (Figure 4.10) techniques to achieve the averaged characterization of the particles. It is known that there is a particle size dependence of the tetragonality in $BaTiO_3$ where particle size below 200 nm present a significant drop in the degree of tetragonality (c/a). The results confirm the stability of the particles at room temperature since their sizes (306 nm for H_24h and 510 nm for nH_72h) correspond to a constant and acceptable c/a.[45]

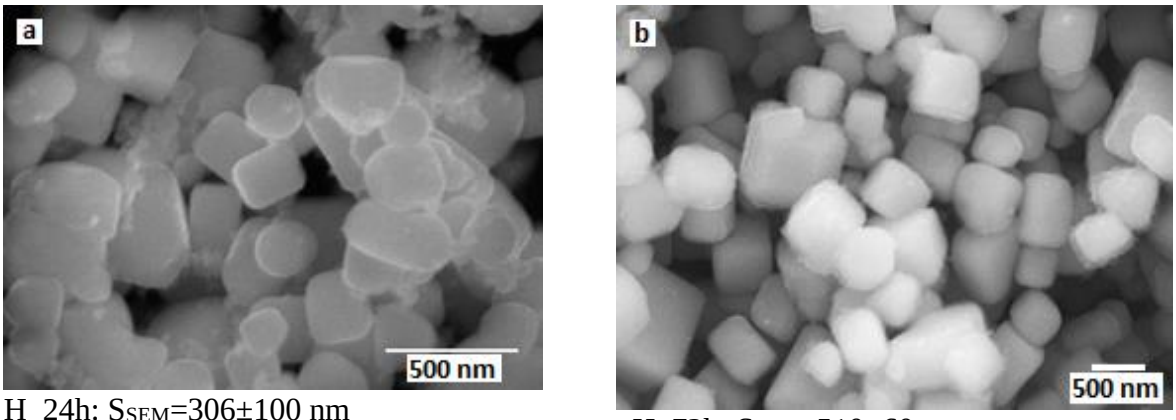

H_24h: S_{SEM}=306±100 nm

nH_72h: S_{SEM}=510±60 nm

Figure 4.8 SEM micrograph of large quantity samples: a) H_24h and b) nH_72h indicating the average size of about 100 particles measured with imageJ.

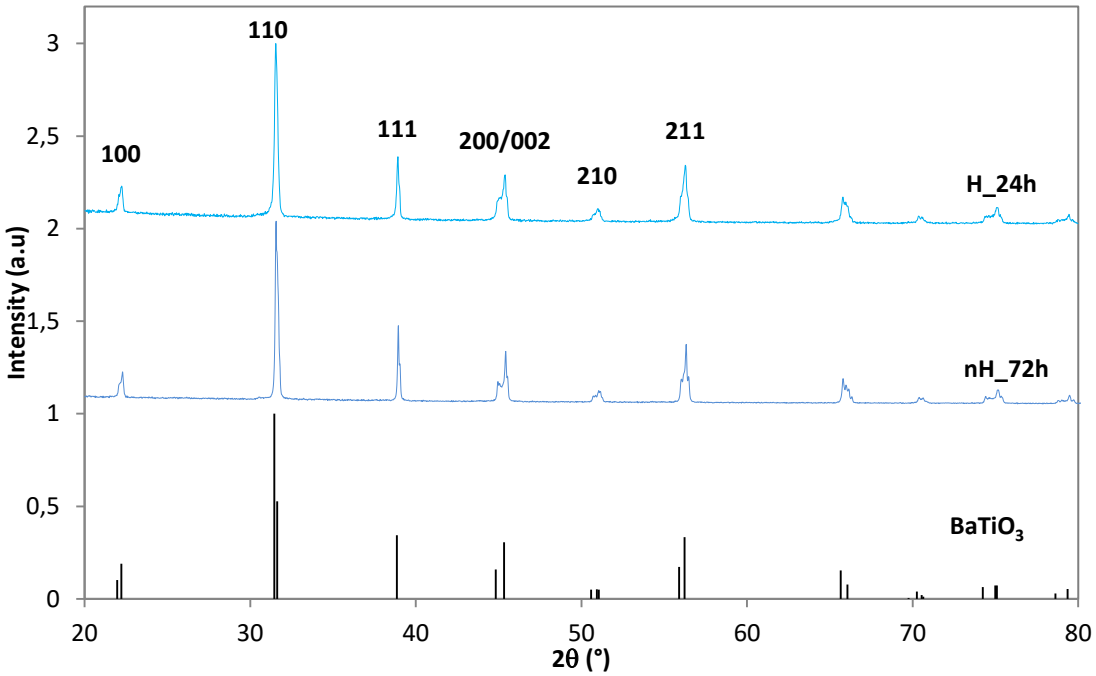

Figure 4.9 Comparison of XRD diffractograms from the large quantity samples: H_24h and nH_72h

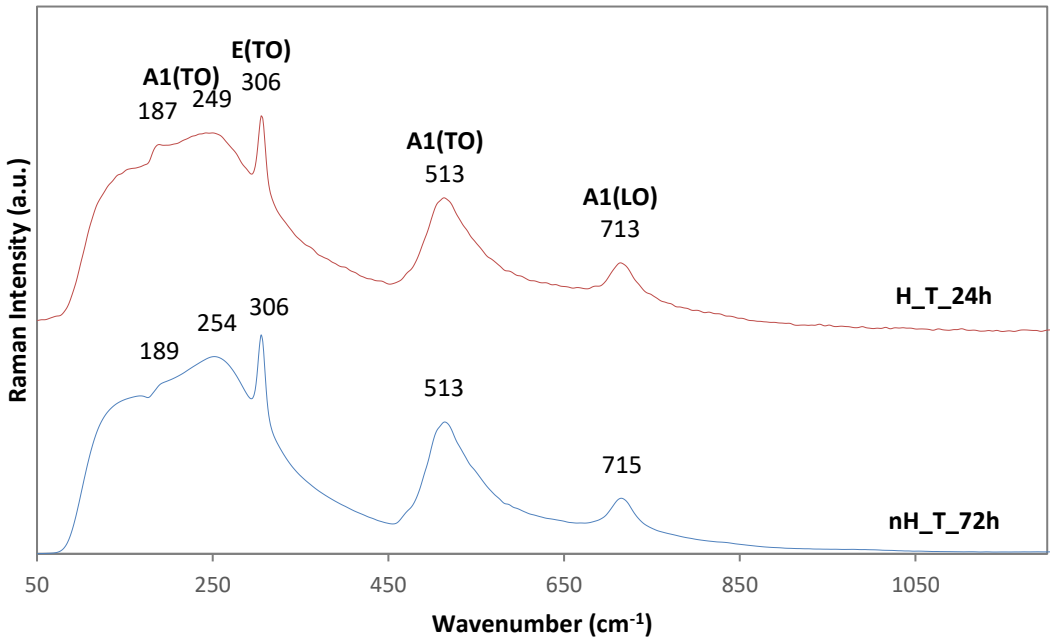

Figure 4.10 Comparison of Raman spectra of the large quantity samples: H_24h and nH_72h.

Chapter 5 Synthesis and characterization of chitosan and $BaTiO_3$ films

In this chapter, the results from the characterization of the prepared free-standing films will be presented. As the particles with H and nH precursors were not significant different (please see Chapter 4 for more detail about the particles), the $BaTiO_3$ obtained with the hydrated $BaCl_2$ ("H") using 24 h of reaction time was selected to incorporate in the membranes. The films were prepared with different ratios of chitosan:$BaTiO_3$ particles, being identified as follows: C (control film), H_1:0.4, H_1:0.5, H_1:0.6, H_1:0.8, H_1:1.5; H_1:2 (chitosan:$BaTiO_3$). Each film has about 0.5 g of chitosan, 0.25 g of glycerol (utilized as a plasticizer) and different concentrations of nanoparticles.

$BaTiO_3$ is used to enhance the dielectric properties of the films and also their response as a piezoelectric composite. The presence of this compound in the blend provides opaque white self-standing membranes while the film C is transparent as shown in Figure 5.1. All the films obtained are easy to bend without cracking, being easily removed from the cast plate. The visual inspection revealed different mechanical behavior of the films, mainly on the hardness and flexibility.

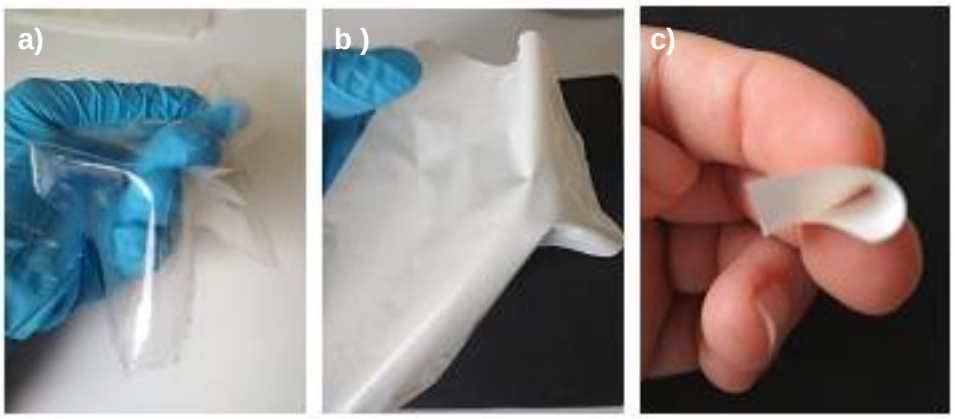

Figure 5.1 Films visual appearance: a) pure chitosan film, b) and c) composite films with increasing quantity of particles.

The increase on the amount of $BaTiO_3$ nanoparticles, to reach the double of chitosan mass, was evaluated by testing with smaller samples as shown in Figure 5.2. This procedure allowed selecting the production conditions of larger size films, expecting that more quantity of particles would increase the electrical properties of the films.

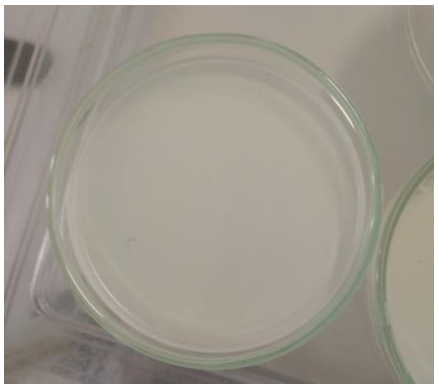

Figure 5.2 Petri test samples

5.1 SEM analysis

The prepared films were morphologically characterized using SEM. Both top and transversal views were analyzed in order to verify the homogeneity of the films and how dispersed were the particles within the bionanocomposite. Figure 5.3 shows the top and cross-sectional micrograph views of the pure chitosan film used as control. The film is homogenous, not presenting any considerable surface defect.

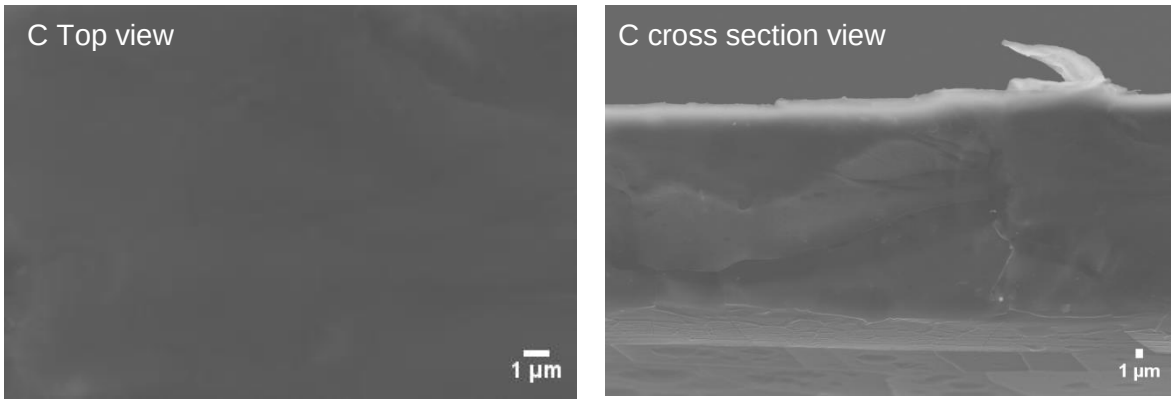

Figure 5.3 SEM micrographs images of the top and cross-section views of the C film.

Figure 5.4 shows SEM micrograph images of the composite films for all the chitosan:$BaTiO_3$ ratio. As it is shown, the particles tend to disperse through the polymer with a certain homogeneity. Apparently, the integration of the particles during the preparation of the film, did not cause any change on the particles shape. It is worth to note that the action of the accelerating voltage of 15 kV in SEM analysis caused some damage in the samples.

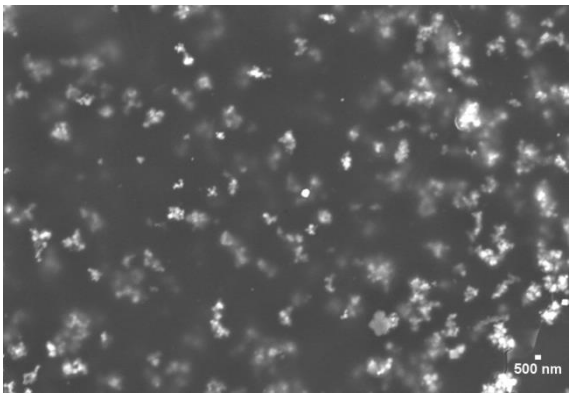

H_1:0.4 TOP

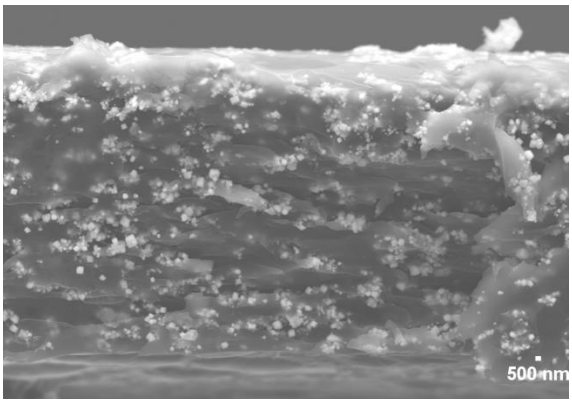

H_1:0.4 Cross Section

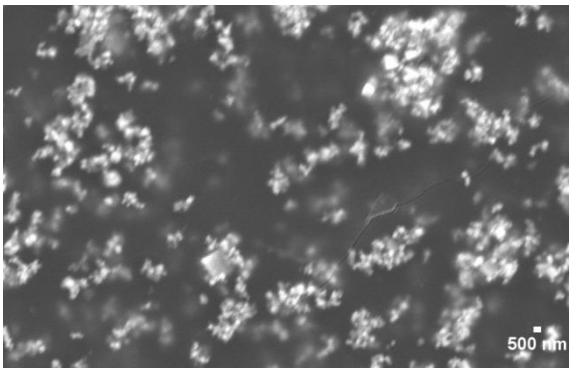

H_1:0.5 TOP

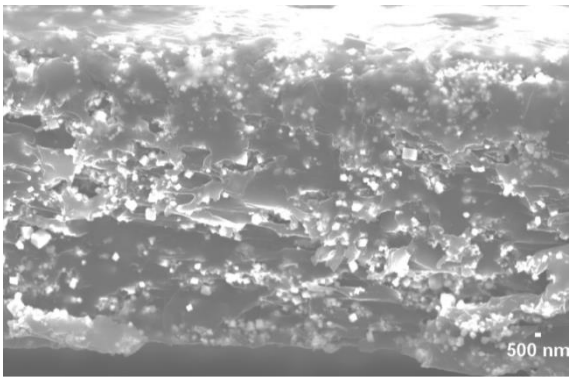

H_1:0.5 Cross Section

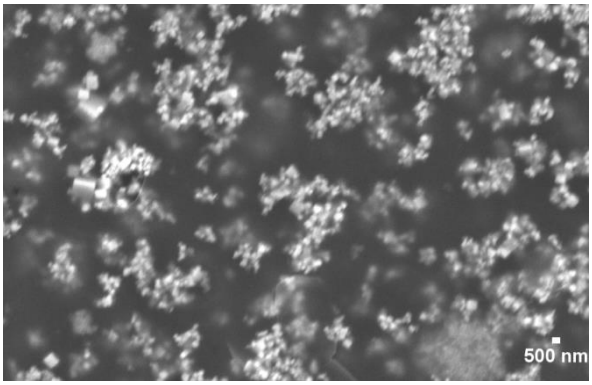

H_1:0.6 TOP

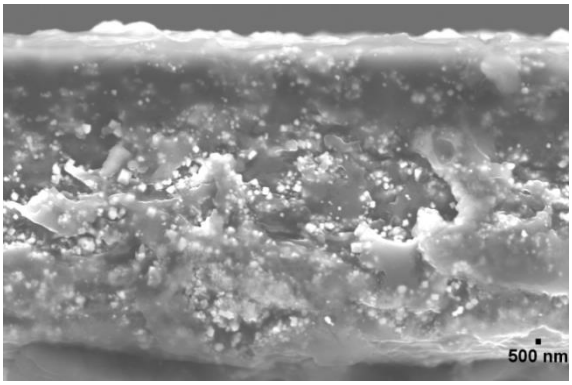

H_1:0.6 Cross Section

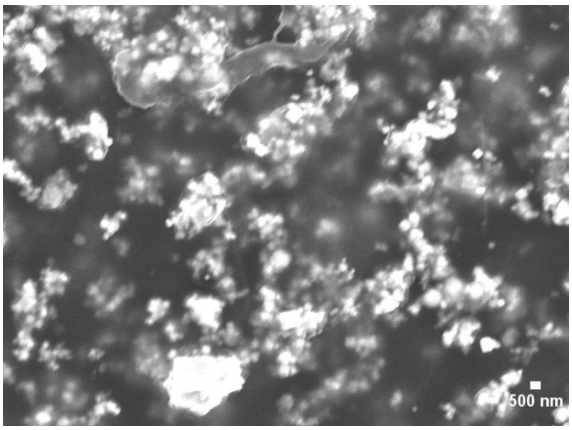

H_1:0.8 Top

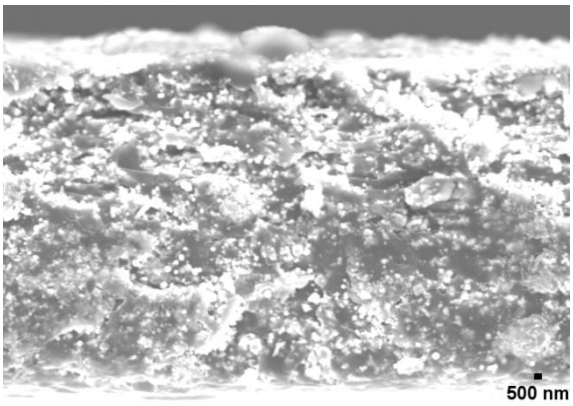

H_1:0.8 Cross Section

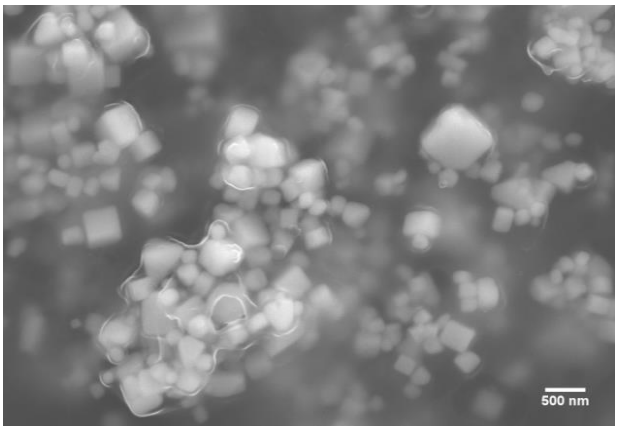

H_1:1.5 TOP

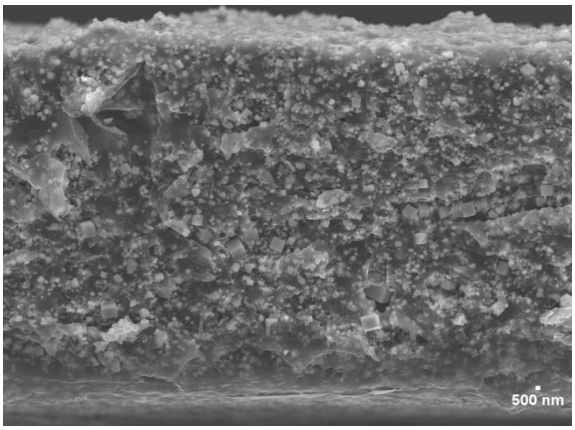

H_1:1.5 Cross Section

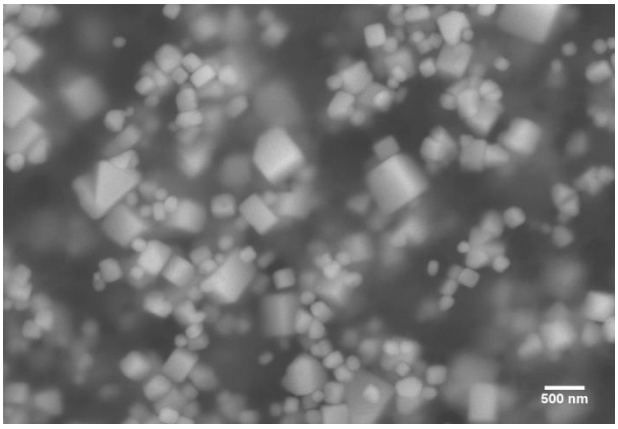

H_1:2 TOP

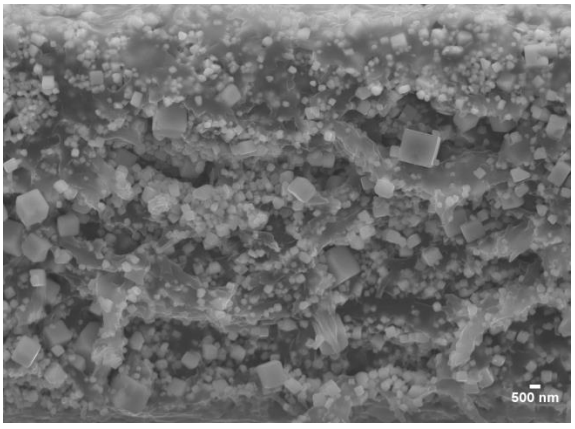

H_1:2 Cross Section

Figure 5.4 SEM micrographs for top and cross-section views of bionanocomposite films H_1:0.4, H_1:0.5, H_1:0.6, H_1:0.8, H_1:1.5; H_1:2.

5.2 XRD and Raman spectroscopy

The XRD and Raman technics were realized to find changes in the particles of $BaTiO_3$ while immersed into the biopolymer (Figure 5.5). As a general view, it is possible to confirm by the XRD diffractograms that $BaTiO_3$ maintain the tetragonal crystallographic phase, which correlates well with the results obtained for the powders. The Raman spectra show that the majority of the films maintain the characteristics peaks with no significant shifting in the representative bands 190, 256, 307, 515 and 715 cm^{-1}(Figure 5.5).

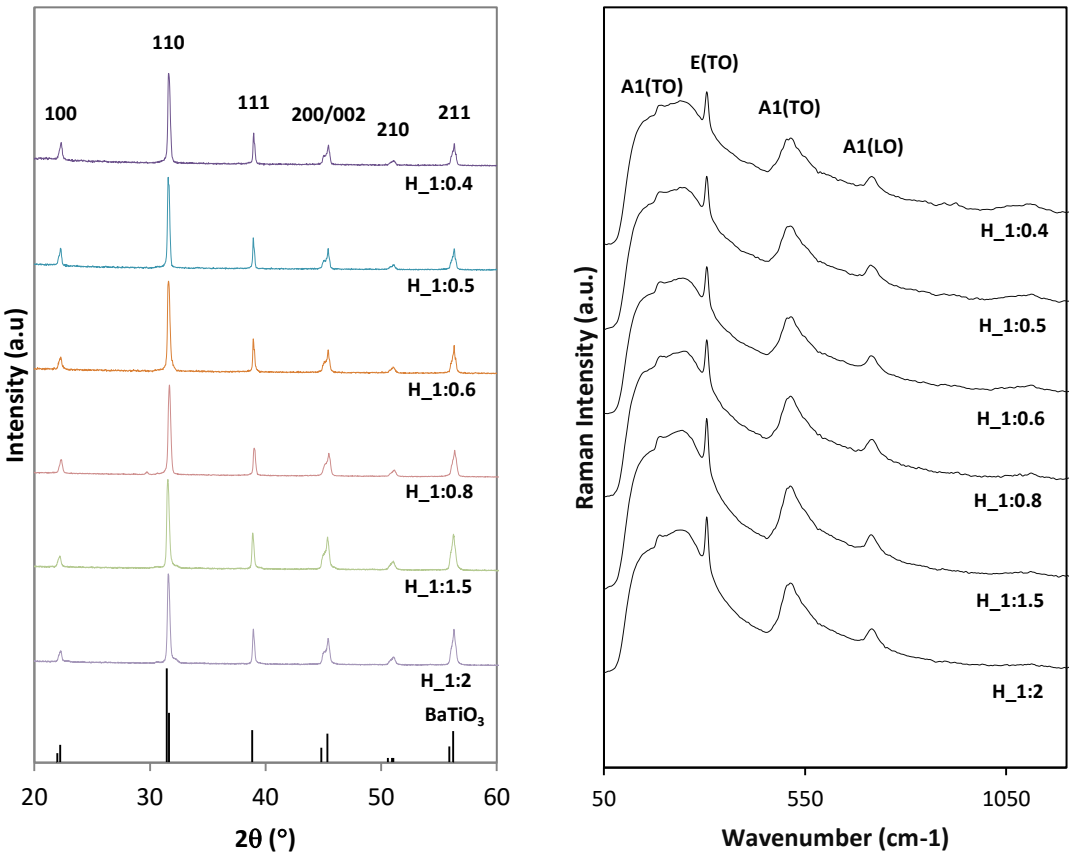

Figure 5.5 XRD diffractograms and Raman spectra of the chitosan and $BaTiO_3$ films.

5.3 FTIR spectroscopy

The Figure 5.6 shows the results of FTIR analyses of all the films obtained with the different ratio of chitosan: $BaTiO_3$. The objective of those spectra was to study the interaction between the biopolymer and the particles. The data was normalized by the highest peak presented, around 1030 cm^{-1}. The functional groups of chitosan film have been indicated as follows: the broad band between 3600 and 3000 cm^{-1}correspond to the O-H and N-H stretching; the following band from 3000 to 2800 cm^{-1} is related to C-H stretching; the peaks below 1750 $cm^{-1}$are attributed to amine groups; those at 1654 cm^{-1} for amide I (C=O vibration), 1556 cm^{-1} for N-H vibration (amide II) and 1283 cm^{-1} attributed to C-N vibration (amide III)[64]; the band at 1374 cm^{-1} correspond to the acetamide group related to the 85% of deacetylation of chitin (according to the manufacturer). The peak at 1409 cm^{-1} is related to de carboxylate group attributed to the presence of residual acetic acid that is used in the preparation of the films for the dissolution of chitosan (please see Chapter 3). The peak at 1031 cm^{-1} is attributed to C-C and C-O vibrations correlated with the structure of chitosan (Chapter 2)[73]. The peak of CO_2 around 2300 cm^{-1} was removed, as it is related to the purge conditions of the spectrometer, and therefore was ignored during the analyze of the samples[58],[74]. Peaks obtained around 506 cm^{-1} are related to the presence of $BaTiO_3$ NPs (blue curve) in the samples. It is noted that the samples with more quantity of particles are also denser and have more defined peaks at this band. The increase of chitosan: $BaTiO_3$ ratio lead to a decrease on the intensity bands related with chitosan, namely the zone between 3600 to 2800 cm^{-1} and 1750 to 1031 cm^{-1}, whereas a decrease of the peak at 506 cm^{-1} was observed.

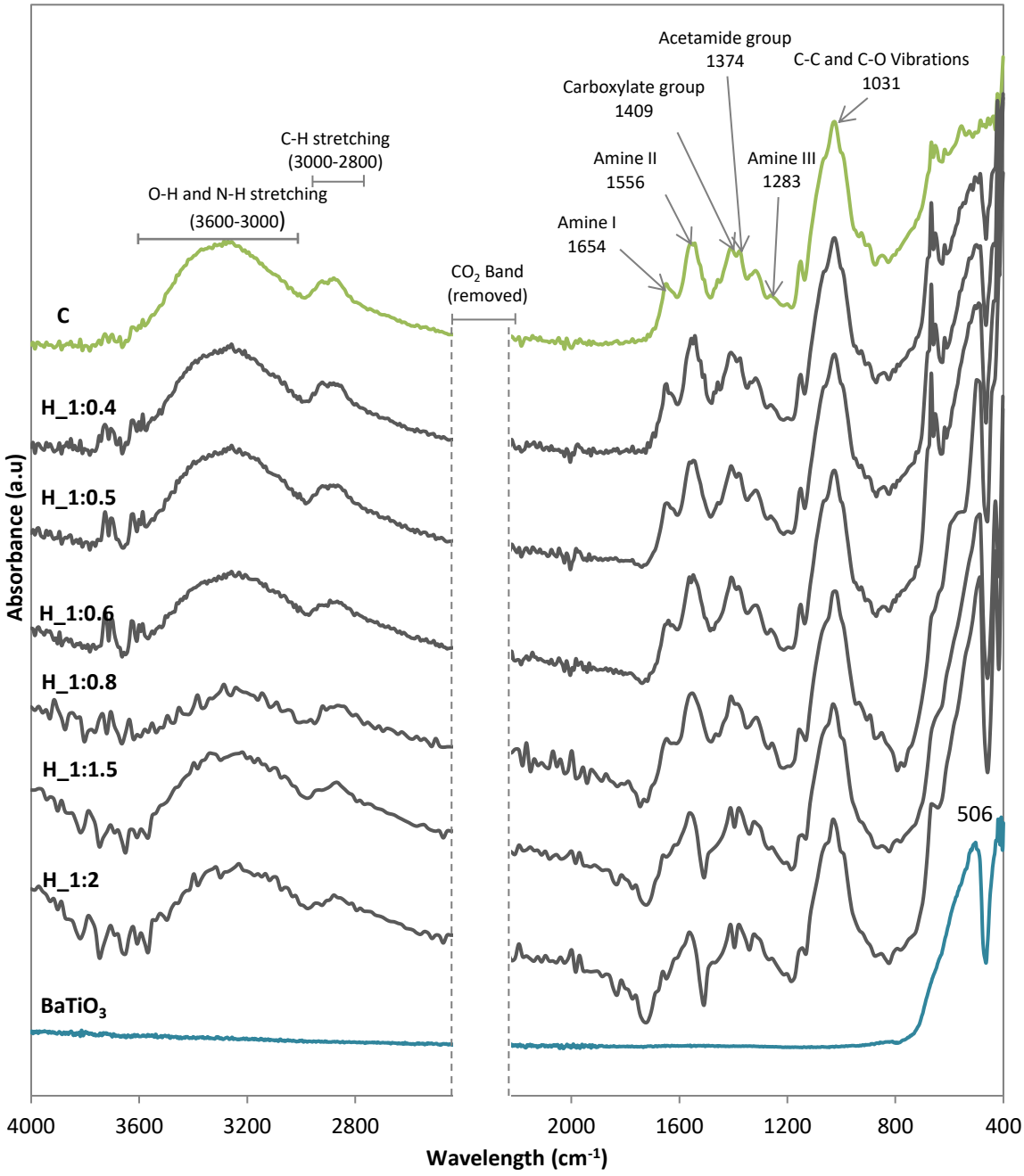

Figure 5.6 FTIR spectra of the chitosan films with different $BaTiO_3$ ratio. The main bands are indicated in the chitosan spectra.

5.4 Physical Properties

The films thickness measurement is presented in Figure 5.7. The thickness varied from 45 µm to 57 µm which are values in the usual order of magnitude of the values reported before for self-standing chitosan films[19], [58], [75]. The samples H_1:0.4 and H_1:2 are slightly thicker than C film, whereas the thickness of other films is not significant different among them (p<0.05).

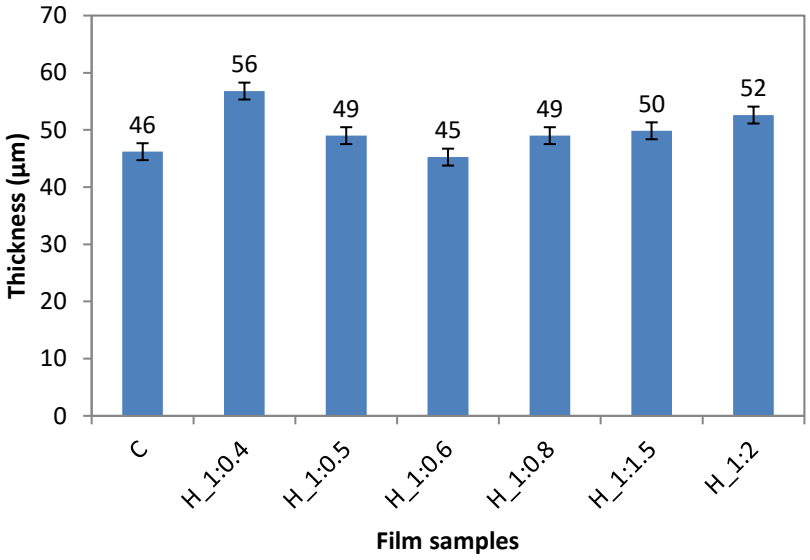

Figure 5.7 Mean thickness of the chitosan films with different $BaTiO_3$ ratio.

Samples of 1 cm^2 were weighted and the density of the films was calculated. The density of the films increases from 1.3 to 2 with the ratio of NPs incorporated **(Figure 5.8),** the highest difference was observed for the films with 1:2 ratio. These values are comparable with similar samples based in chitosan biopolymer reported before by Rajala *et al*[65] and Hänninen *et al.*[76]

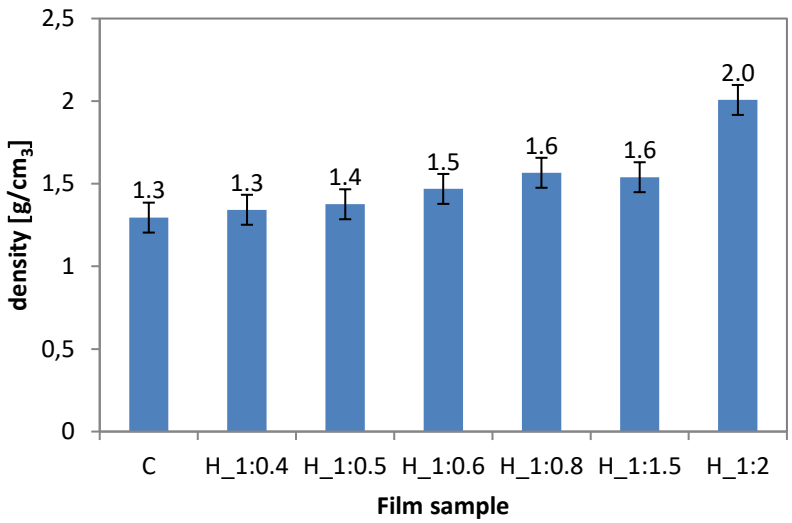

Figure 5.8 Mean density of the chitosan films with different $BaTiO_3$ ratio.

Contact angle

The surface hydrophilicity of the films is an important parameter to evaluate the behavior of the films in the presence of water. This measurement was applied to all films in the top and bottom surfaces, being the bottom surface, the one that was in contact with the acrylic plate during the solvent evaporation. Figure 5.9 shows the photographs of the ultrapure water drops in both surfaces of each film. In general, they have a similar behavior, forming a defined spherical cap on the film surface with different contact angles.

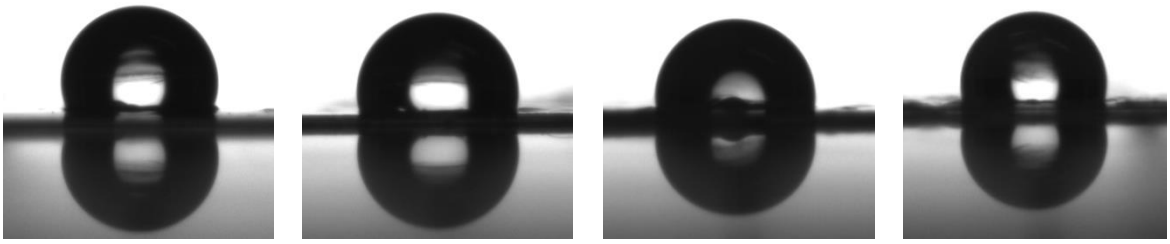

C: TOP | C: BOTTOM | H_1:0.4 TOP | H_1:0.4 BOTTOM

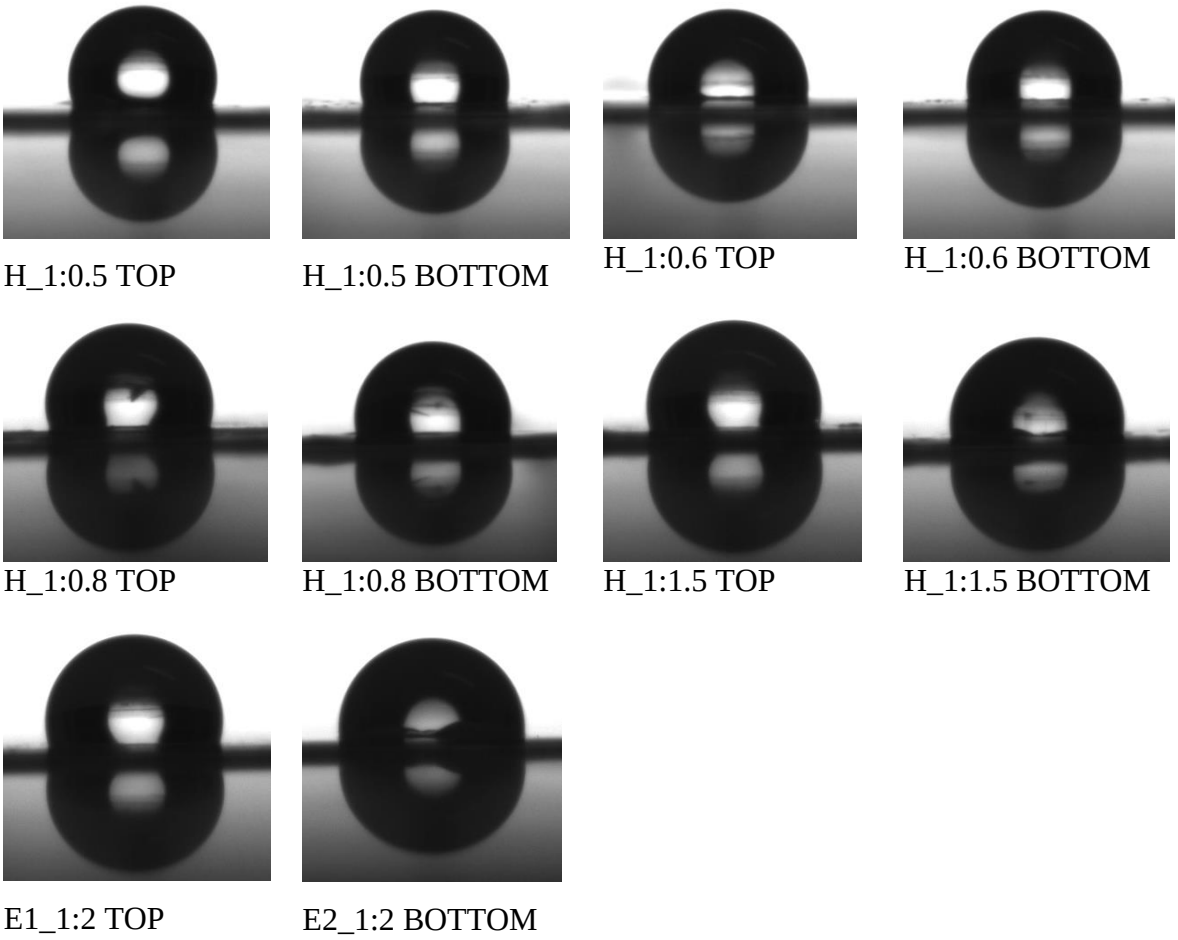

Figure 5.9 Photographs of the dispensed drops in samples (TOP and BOTTOM) for chitosan films with different $BaTiO_3$ ratio.

The plot of Figure 5.10 quantifies the variation of the contact angle by the incorporation of particles into chitosan-based films. The contact angles of bottom and top surfaces with water in pure chitosan film do not present significant differences. Nevertheless, with increasing particles concentration, the films tend to be more hydrophilic in the bottom surface in comparison to the top one (more evident on the films H_1:1.5, H_1:2). Among film samples, the top surfaces do not show significant differences ($p<0.05$). However, in the bottom surface of the films become significantly more hydrophilic. Three groups of samples with three types of behaviors are identified according to the quantity of barium titanate particles added to chitosan. Low quantities of particles (up to 0.5) do not modify the hydrophobic behavior of the bottom surface. Medium addition of particles (between 0.5 and 0.8) started to decrease the hydrophobic character of the films. For high quantity of

particles (higher than 1.5), the films became more hydrophilic in the bottom surface. The theoretical density of the barium titanate particles is 6.02 g/cm³ tending to deposit into the bottom surface turning the surface more hydrophilic. The top surfaces of all films did not change significantly as their compositions are very similar to the pristine chitosan film.

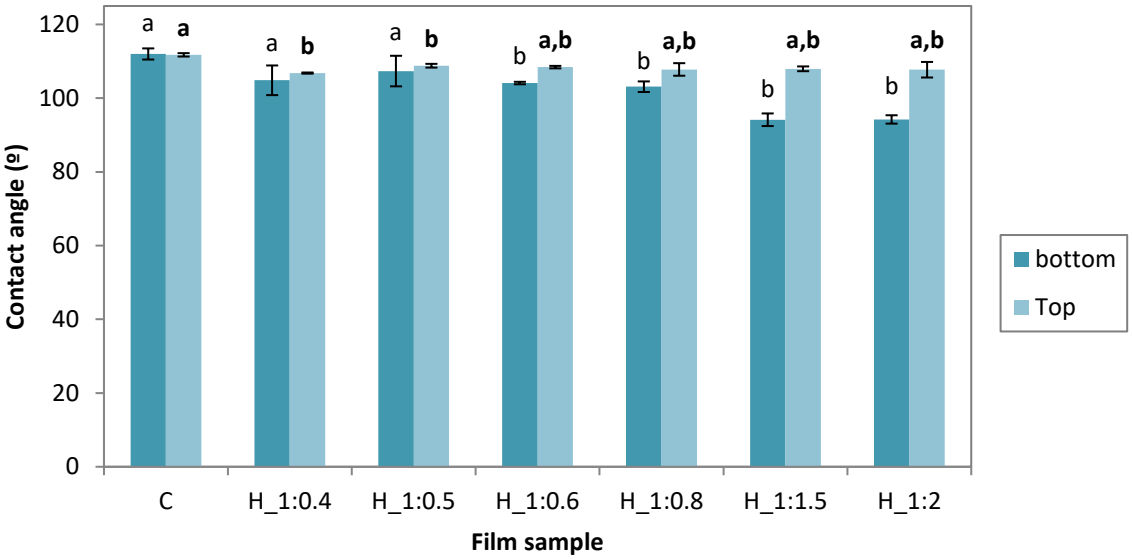

Figure 5.10 Mean values of contact angles for chitosan films with different BaTiO3 ratio in Bottom and top surface. Different superscript letters represent statistically different values (*p*<0.05).

Moisture content

Figure 5.11 shows the moisture content of the samples. In general, the humidity value decreased significantly ($p<0.05$) as the $BaTiO_3$ nanoparticles were incorporated into the chitosan-based films. The presence of the particles is also traduced in less amount of chitosan. This implies less hydroxyl and amino groups and limits the interaction between the polysaccharide and the water by hydrogen bonding, resulting in a decrease of moisture content in the films[77]. There is again a marked difference between three specific ratios classified before (low, medium, and high).

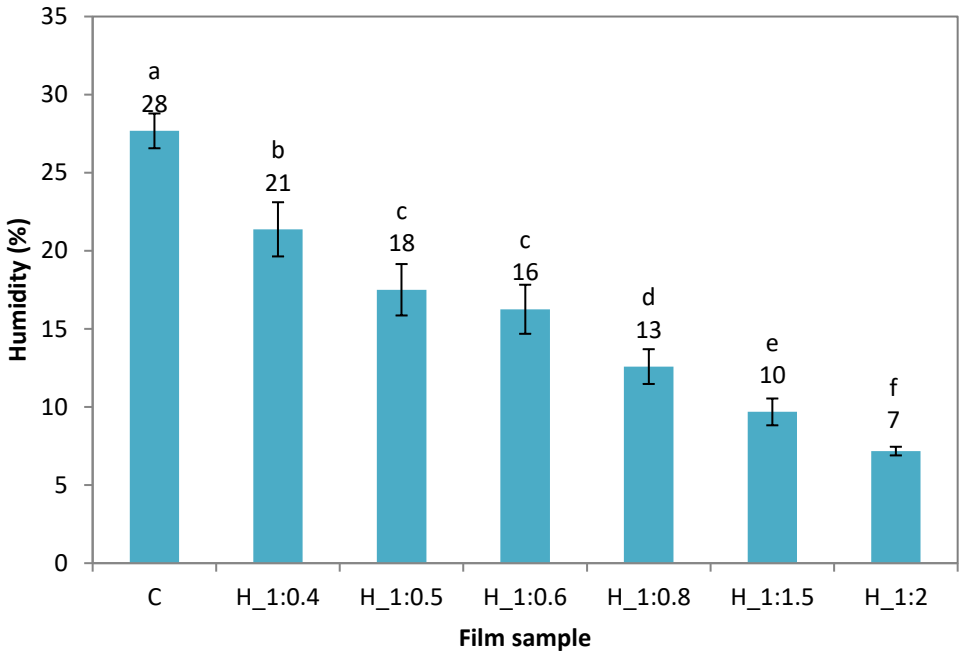

Figure 5.11 Humidity percentage for chitosan films with different $BaTiO_3$ ratio. Each letter represents significantly different values (p<0.05), numbers describe the mean calculate value.

Solubility

The solubility was determined after immersing the films in water for seven days. Figure 5.12 shows that the solubility decreases with the increasing of the $BaTiO_3$ content in the samples. As chitosan is not soluble in water the mass loss might be related with diffusion of glycerol molecules to the water medium. Therefore, when high quantity of particles is incorporated into the films, the solubility is reduced. The diffusion of glycerol may be avoided by the presence of the particles due to the interaction between them, as well as with chitosan. This result allows to infer that $BaTiO_3$ particles are homogenously distributed in the chitosan and are interacting with the matrix since they not diffuse to the water.

Low values of solubility and humidity in the samples could be favorable for sensor or actuator applications due to their effect in the durability of the material which is one of the important requirements for these devices[64]. Nevertheless, it could also represent a drawback as the time for degradation increase in terms of waste treatment.

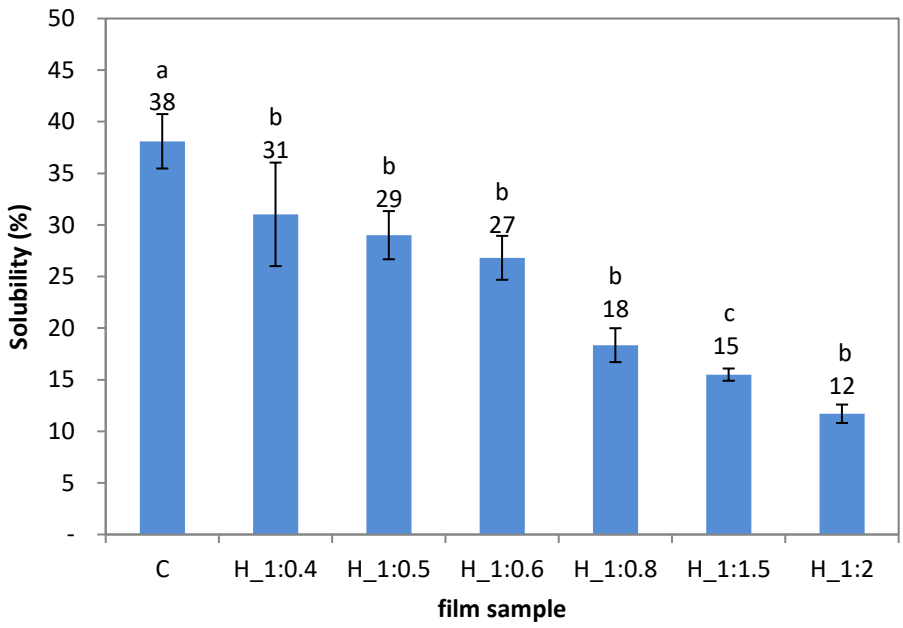

Figure 5.12 Solubility of chitosan films with different $BaTiO_3$ ratio after the immersion in water for seven days. Each letter represents significantly different values (p<0.05).

5.5 Mechanical properties

Aiming to characterize the mechanical properties of the prepared films, values of Young modulus (Y), elongation at break (EB) and tensile strength (TS) were obtained from the analysis of stress-strain curves. The mechanical properties are useful to study the resistance of the material to external forces. Y values present a bell-shaped distribution (Figure 5.13) were the highest results are presented for films with a medium ratio of particles (H_1:0.5, H_1:0.6). The C and H_1:0.4 present Y around 200 MPa which is typical for this kind of films[58], [77]. The Y decrease again for films with higher $BaTiO_3$ ratio, greater than 1:0.6. Regarding these results, it is evident that the incorporation of $BaTiO_3$ to the chitosan-based films have different influences on the films according to the concentration. Up to 1:0.6 chitosan: $BaTiO_3$ ratio, the particles enhance the stiffness of the films and above this ratio, the particles increase the elasticity of the films, i.e. the film changes its shape easily with small loads.

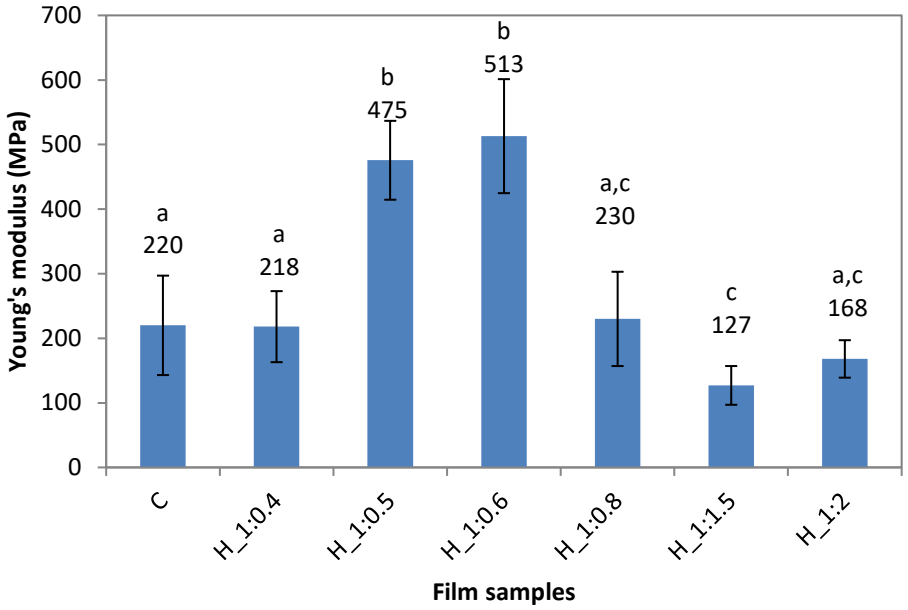

Figure 5.13 Young modulus calculated from stress-strain curves for chitosan films with different $BaTiO_3$ ratio.

The tensile strength describes the maximum force that the films are capable to support before breaking. The Figure 5.14 shows a special behavior, films with higher ratios than 1:0.5 are significantly more resistant to the force applied than films with lower content of nanoparticles and pristine one ($p<0.05$). This result revealed that $BaTiO_3$ nanoparticles are interacting with chitosan structure strengthening the film, which is in accordance with the results obtained for the films solubility (lower solubility for higher chitosan:$BaTiO_3$ ratio).

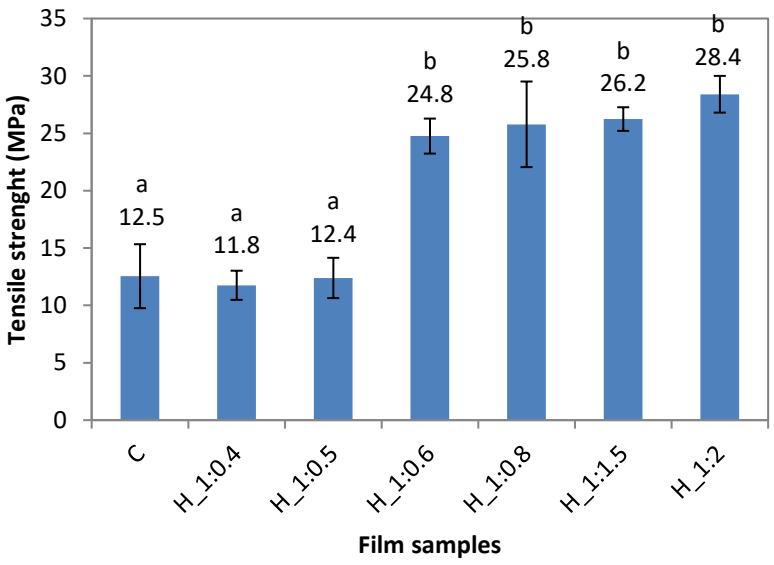

Figure 5.14 Tensile strength calculated from stress-strain curves for chitosan films with different $BaTiO_3$ ratio.

Figure 5.15 shows the ability of the films to extend when stretched (plasticity). In this case it appears to have an inversed bell-shaped curve, where the lowest value is reached in the films with 1:0.5 ratio. The films elongation increased for higher chitosan:$BaTiO_3$ ratio, reaching a stable value for the films with 1:0.7 to 1:2 ratio. The highest elongation at break of the films with the higher content of nanoparticles revealed an increase of films plasticity. Once more, this confirms an interaction between chitosan and $BaTiO_3$.

Overall the chitosan-based films with higher ratios of $BaTiO_3$ particles are more elastic, plastic, and resistant to stress, which are suitable mechanical properties to be applied as flexible sensors for biomedical applications.

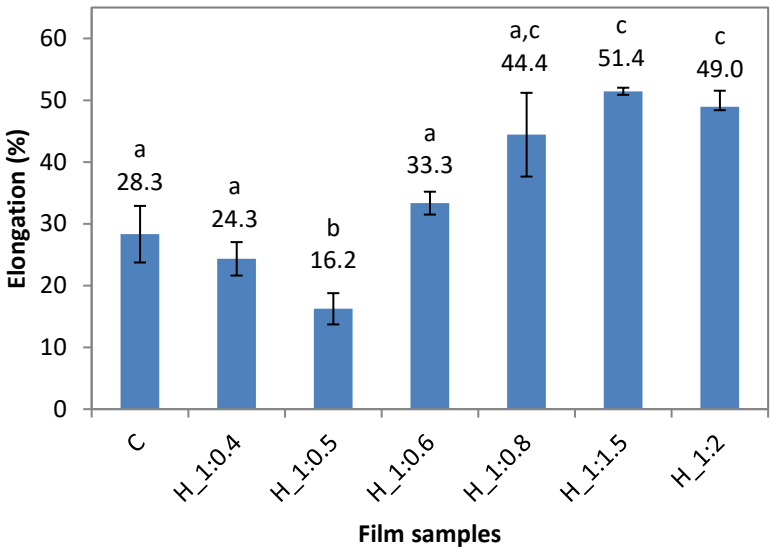

Figure 5.15 Elongation percentage calculated from stress-strain curves for chitosan films with different $BaTiO_3$ ratio.

5.6 Dielectric characterization

Samples were coated with gold electrodes. The continuity of the Au electrode coat was measured and was not homogenous. Therefore, new electrodes of conducting silver paint were applied for new measurements performed with the objective of getting more reliable results. Figure 5.16 shows an example of control samples and composite ones.

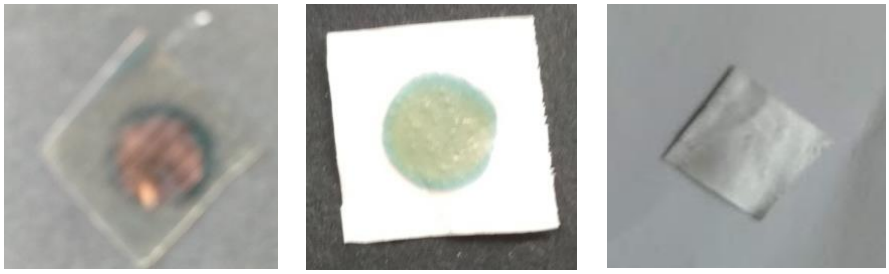

a **b** **c**

Figure 5.16 Photo image of the prepared samples with electrode: a) chitosan control film; b) sample with BT nanoparticles; c) Composite sample with Ag electrode.

The electric behavior of chitosan, and chitosan-$BaTiO_3$ films, was obtained by measuring their dielectric permittivity using the LCR meter. The real permittivity (ε') and the loss factor (ε'') were calculated from the obtained relative permittivity (ε_r) and the dielectric losses known as Tan δ, using the following relations:

$$\varepsilon^* = \varepsilon_r = \varepsilon' - i\varepsilon'' \tag{5.1}$$

$$Tan\ \delta = \frac{\varepsilon''}{\varepsilon'} \tag{5.2}$$

ε' is related to the energy stored reversible in the material while ε'' describes the energy dissipated per cycle.

Figure 5.17 and Figure 5.18 shows the real and imaginary behavior obtained for a rank of frequencies from 100 Hz to 1 MHz, respectively. The theoretic curve for a dense pellet of BT is displayed in Figure 5.17 for comparison proposes. The real permittivity decreased with the increasing of frequency in all the samples which is a normal behavior of dielectrics materials. High values of permittivity at low frequencies are usually related to interfacial polarization of the dielectric (rise by the grain boundaries and interfaces between different materials) and electrode effects observed in polycrystalline structures, there is also a contribution of different mechanisms of polarization as dipolar moments and free space charges. As it can be observed the behavior in the theoretical curve is very different as it is completely excluded any porosity.

The permittivity of chitosan is around 300-500 at low frequencies (f < 1 kHz) and the values increase for composite films where the incorporation of $BaTiO_3$ particles increases the permittivity. At relatively high frequency (f>10 kHz) the dielectric constant showed differences for all films being C the one with the lowest value. For f=100 kHz the dielectrics constant of chitosan film was 33 which matches with reported values of chitosan films at this frequency[23]. Adding $BaTiO_3$ increased the relative permittivity value from 33 to 60 and 150. The rise in this values could be the result of the principle of combined action of two phases[78] considering the high permittivity of barium titanate and its stability along the frequency (ε~1000 at f=10-10^7 Hz). The sample H_1:1.5 shows a higher value and the one with more concentration of NPs (H_1:2) shows a reduction of its ε'

which could be due to the agglomeration of particles and consequently formation of pores between $BaTiO_3$ grains in some sections or the reduction in the contribution of dipolar polarization.

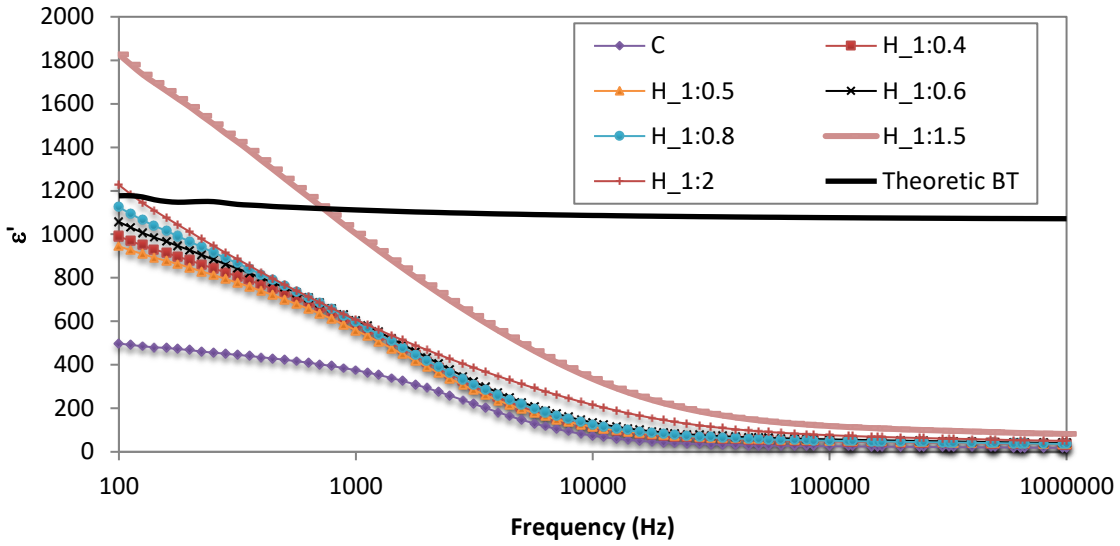

Figure 5.17 Real permittivity (ε') of samples C, H_1:0.4, H_1:0.5, H_1:0.6, H_1:0.8, H_1:1.5, H_1:2 measured with LCR meter and theoretic BT.

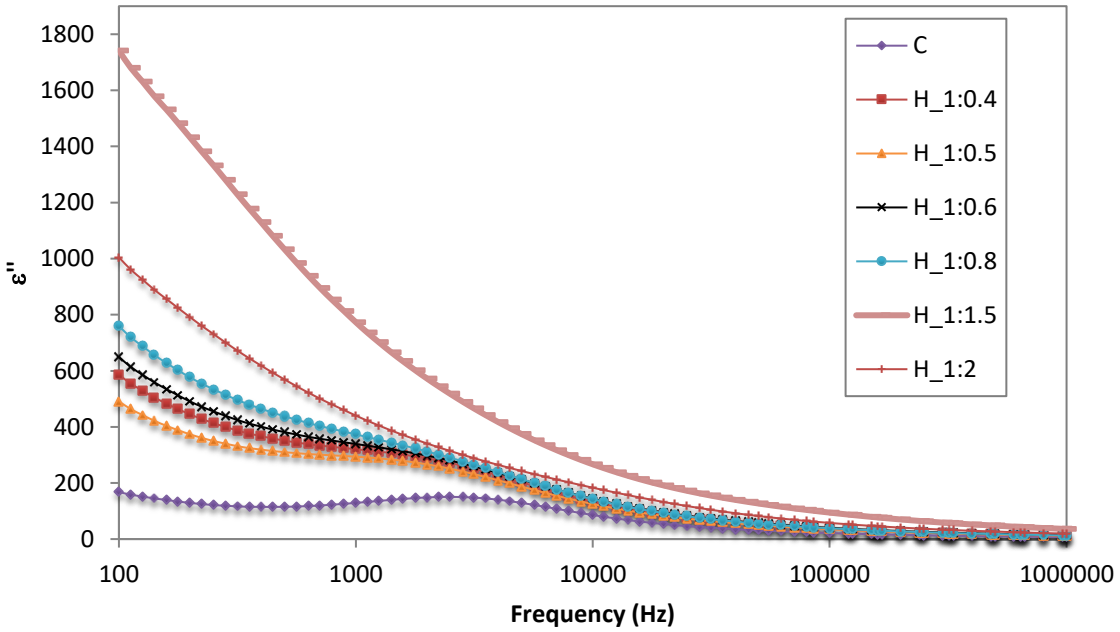

Figure 5.18 Re loss factor (ε'') of samples C, H_1:0.4, H_1:0.5, H_1:0.6, H_1:0.8, H_1:1.5, H_1:2 measured with LCR meter.

The imaginary part of dielectric permittivity is shown in Figure 5.18. It is mainly related with the conductivity of the samples, in this case the decrease of permittivity along the frequency corresponds to the expected behavior for heterogeneous systems characterized by dielectrics with different conductivities as in the fabricated biocomposite[79]. It is explained by the Debye-like relaxation process which is produced by the accumulation of charges at the boundaries of the grains when the electric current passes through them under an applied electric field[80]. Furthermore, it also explains the increase of the values with the addition of NPs and the consequent increase in energy losses.

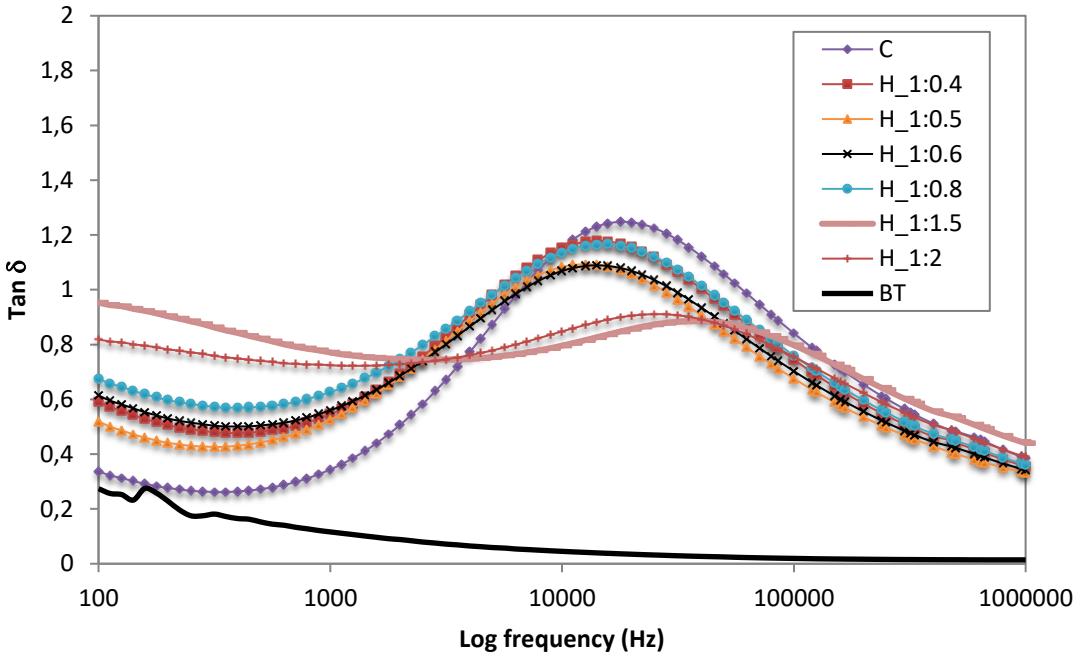

Figure 5.19 Dielectric loss (Tan δ) of samples C, H_1:0.4, H_1:0.5, H_1:0.6, H_1:0.8, H_1:1.5, H_1:2 measured with LCR meter.

The dissipation factor (Tan δ) related to the relaxation time reaches its major value around 10 kHz for all thick film samples (Figure 5.19). There is a shifting to lower frequencies for films with 0.4 to 0.8 ratios of $BaTiO_3$ NPs in relation to the control sample. For samples with higher $BaTiO_3$ concentration (H_1:1.5 and H_1:2), there is a decrease of losses and a shifting of the peaks from 17 kHz (C) to 35 kHz. According to Debye theory there is an inverse relation between polarizability and time of relaxation, the obtained results suggest a

decrease in relaxation time for films with higher concentrations, therefore, these samples could be easier to polarize due to the main contribution of dipolar polarization mechanism.

The permittivity is not a constant value and it depends of other factors as temperature, moisture, and type of material[60]. This effect is showed in Figure 5.20 where dielectric constant of sample H_1:0.4 was tested for several values of temperature at 1 kHz.

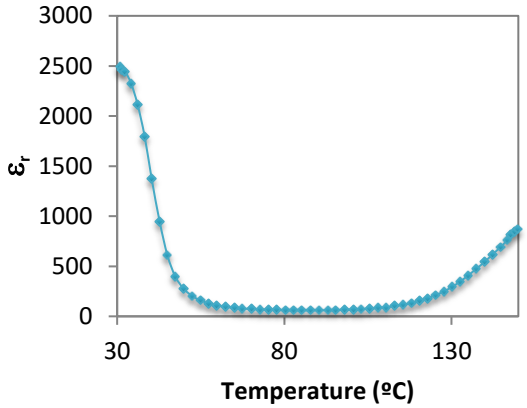

Figure 5.20 Dependence of relative permittivity with temperature for H_1:0.4 film.

Poling process

It is known that the poling process is the most difficult stage while trying to characterize ferroelectrics[81], due to all the parameters that could affect measurement and results. The obtained films showed high dielectric losses, hence the favorable values of permittivity could not be enough to an acceptable piezoelectric response.

The corona poling method was carried for some samples (H_1:0.4, H_1:0.8, H_1:1.5 and H_1:2). Nevertheless, there was any piezoelectric response obtained by the available equipment in the laboratory. Then The hysteresis loops were obtained for the sample with the major concentration (H_1:2) and the obtained result does not correlate with a ferroelectric material behavior. As shown in Figure 5.21.a. The E-P loop does not present any contribution to domain switching. In the I-E loop the current is proportional to the applied field, which confirms the contribution from dielectric permittivity and electric conductivity obtained in dielectric characterization. As the E-P loop is characteristic of resistances, the electric conductivity of the material should be the one with major

contributions in this sample. It is worth to note that other factors as temperature, texture, grain size and frequency are also variables that affect the hysteresis loops of dielectrics.

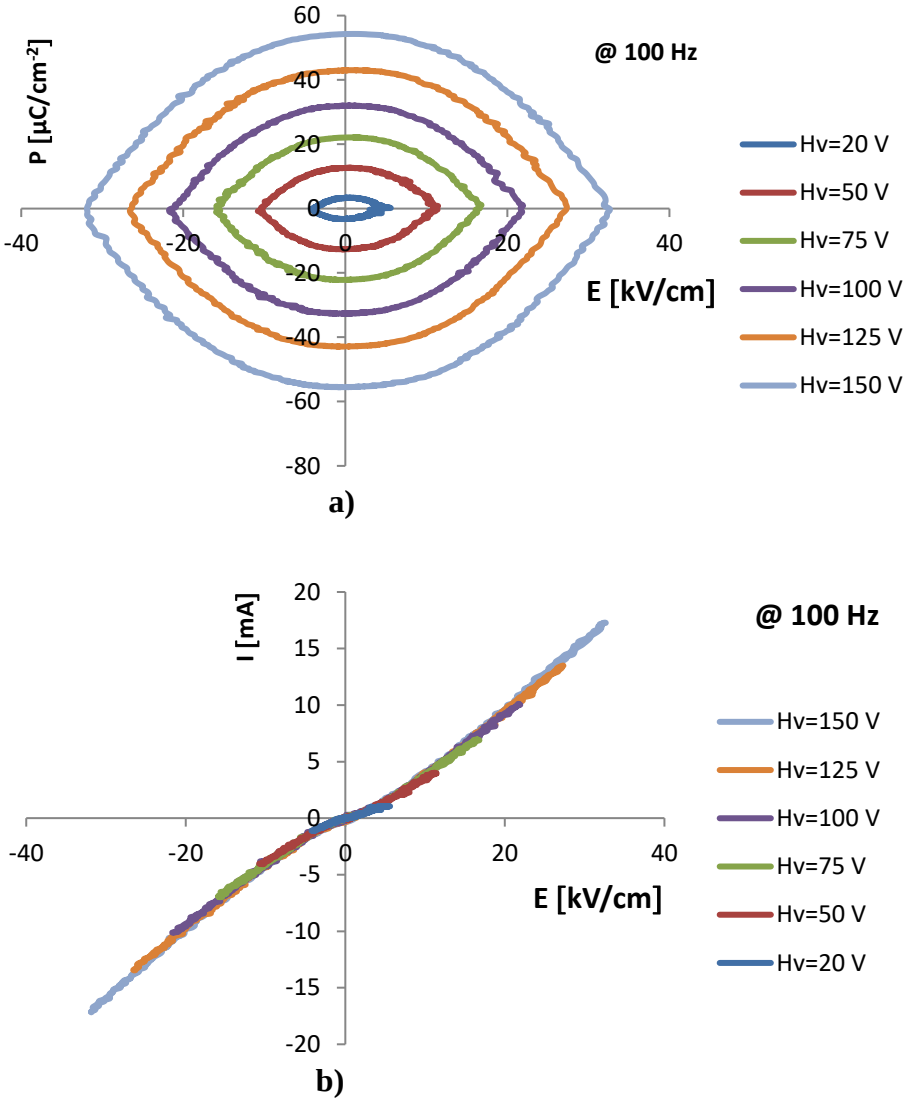

Figure 5.21 a) P-E hysteresis loop for composite sample H_1:2 at 100 Hz. b) I-E hysteresis loop for composite sample 1:2 at 100 Hz.

PFM

As we did not obtain a piezoelectric behavior of the film at macroscale, we tried to measure it at nanoscale using PFM technique. Therefore, a local analysis of piezoelectric response was performed with PFM for C and H_1:2 samples.

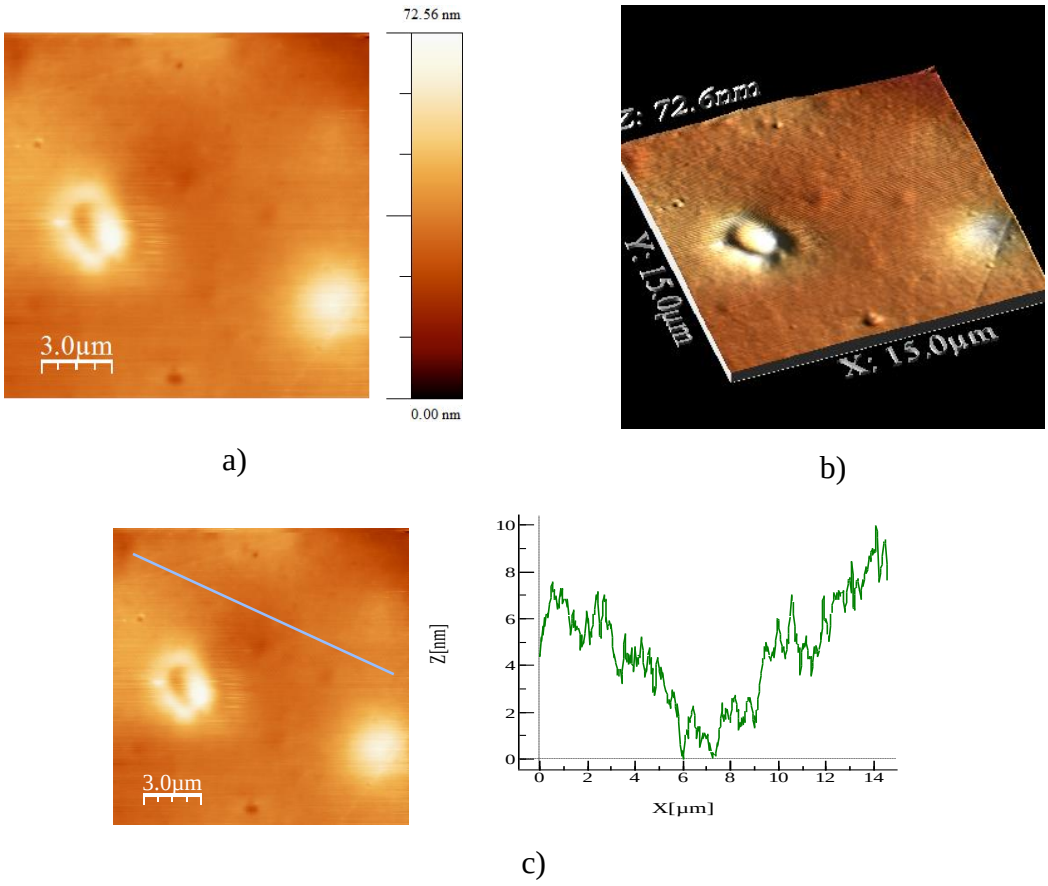

Figure 5.22 Topography images of chitosan film (C) and height profile.

In the Figure 5.22.a) and b) the top and 3D view of the C film are presented. The obtained mean topography is RMS=4.5 nm, showing clearly the smooth surface of the control film. The small defects could be due to remaining air bubbles during the casting process. The piezoresponse of chitosan films is shown in Figure 5.23. It is clear a total absence of domain contrasts in the image that proves the non- piezoelectric character of this biopolymer.

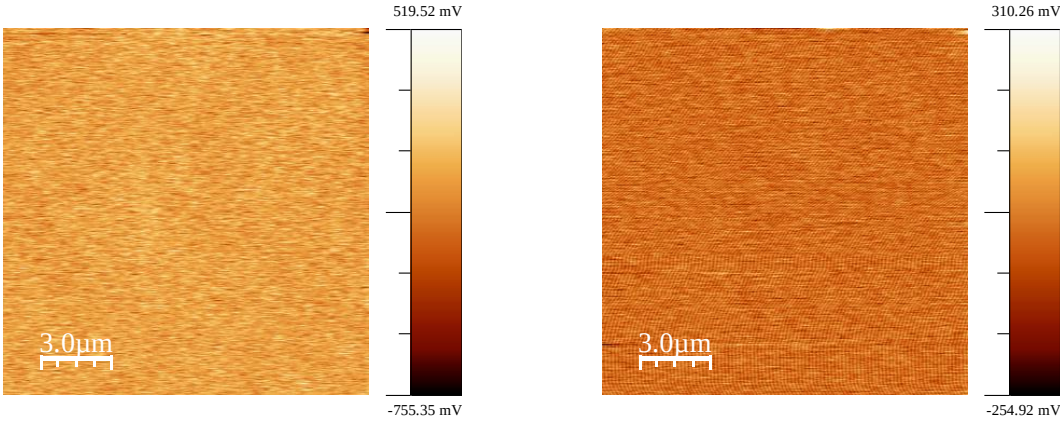

a) b)

Figure 5.23 PFM images of the pure chitosan films measured a) out-of-plane d_{33}, b) In-plane d_{15}

A specific voltage was applied to obtain the KPFM response of the pure chitosan film. The obtained result shows some remaining charges at the surface (Figure 5.24.b). These charges could be caused by the presence of voids in the polymer and could be related with the electret behavior referred before (chapter 2).

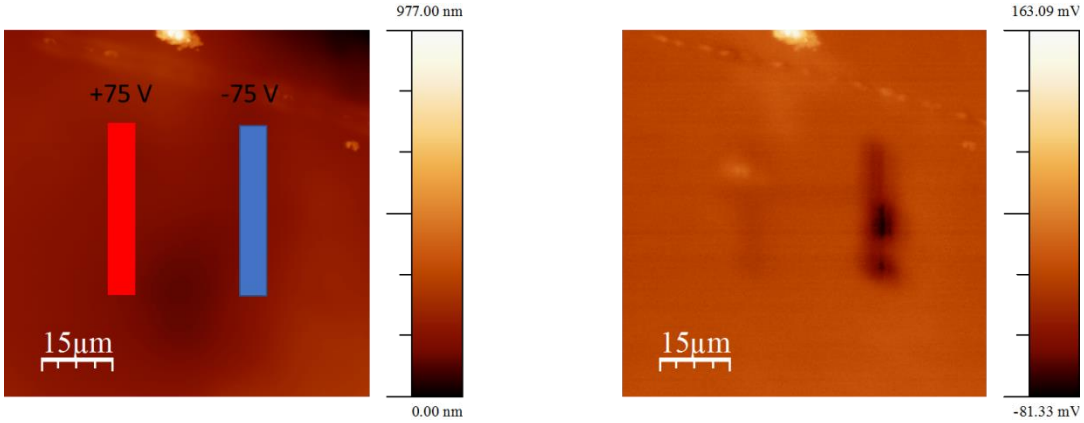

a) b)

Figure 5.24 AFM topography a) Kelvin probe force microscopy (KPFM) after application of a voltage of +75 V and -75V in two different rectangle (b) Image of the result after KPFM.

The Figure 5.25 shows the possible behavior of the sample: an applied field causes the formation of charges around the free spaces allowing the generation of dipoles that may be represented in the remaining polarization of the sample.

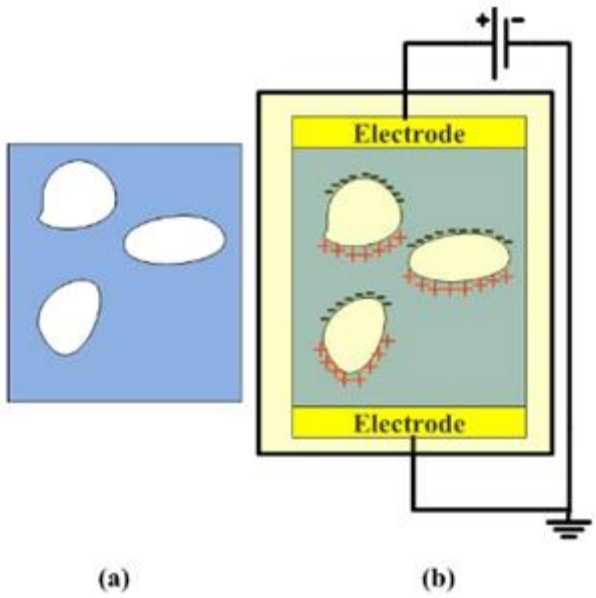

Figure 5.25 Diagram of piezoelectricity in voided charged polymers: (a) a polymer before charging and (b) the electrode poling process for forming the trapped dipoles [70]**.**

The H_1:2 sample (the one with more quantity of $BaTiO_3$ NPs) was also studied. Figure 5.26 shows the topography images for the H_1:2 sample. The calculated RMS is 140 nm and correspond to the TOP face. It is note that adding $BaTiO_3$ NPs to the chitosan-based matrix significantly increases the roughness of the film. The particle size was also confirmed being approximately 310 nm.

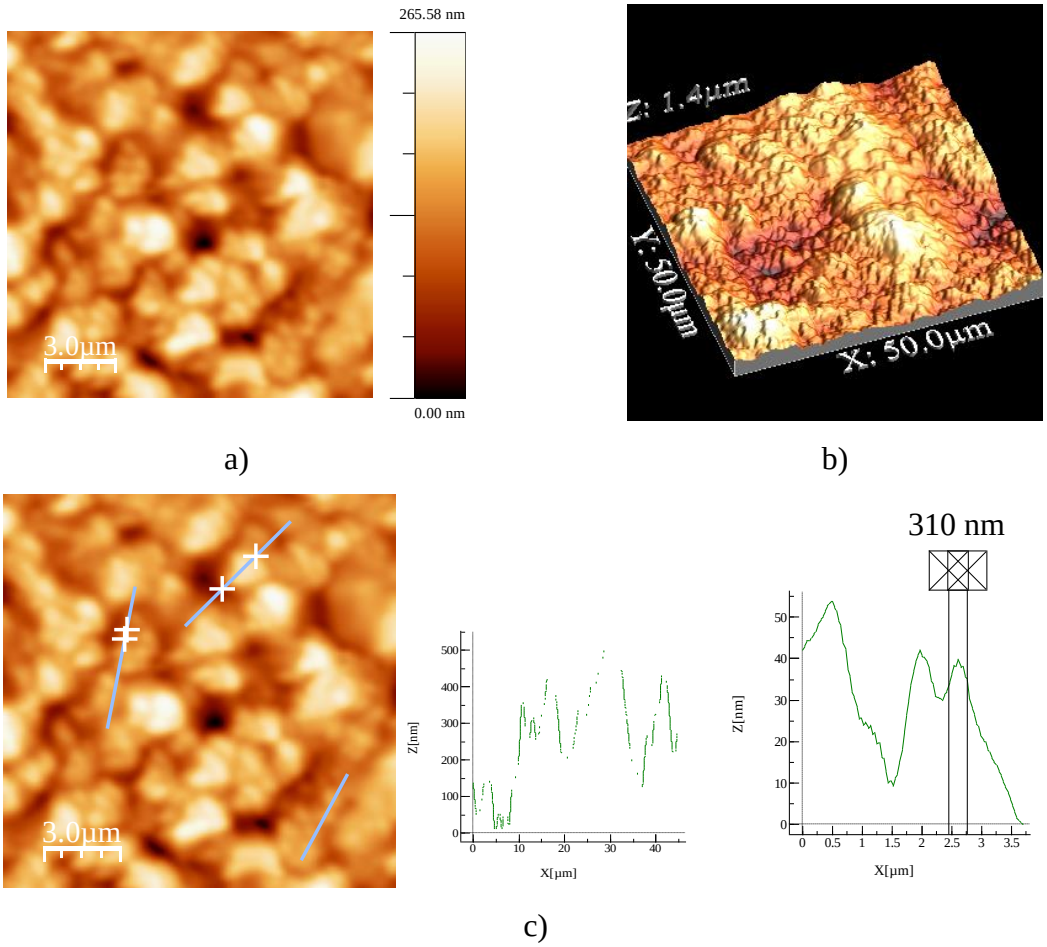

Figure 5.26 Topography of H_1:2 film: a) plane view, b) 3D view, c) Profile of the height values along the film in the marked area of 2D AFM topographic image and identification of particle size.

The observed piezoelectric contrast is attested to the surface piezoelectricity due to the flexoelectric effect (Figure 5.27) .

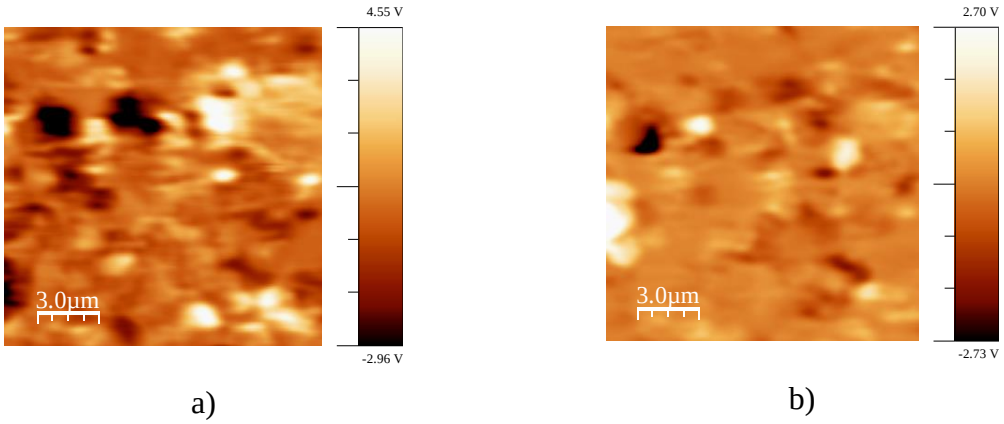

Figure 5.27 Piezoresponse PFM in 1:2 sample: a) out-of-plane d_{33} and b) In-plane d_{15}.

As there was a piezoelectric response, the attempt to do the switching was performed. The results were not really clear, and it was not possible to obtain a well-defined hysteresis loop. Some areas of the sample showed changes after poling, these results are signaled in

Figure 5.28. It could be that the switching corresponds just to the particles of BaTiO3, taking into account the behavior of the polymer.

a)

b)

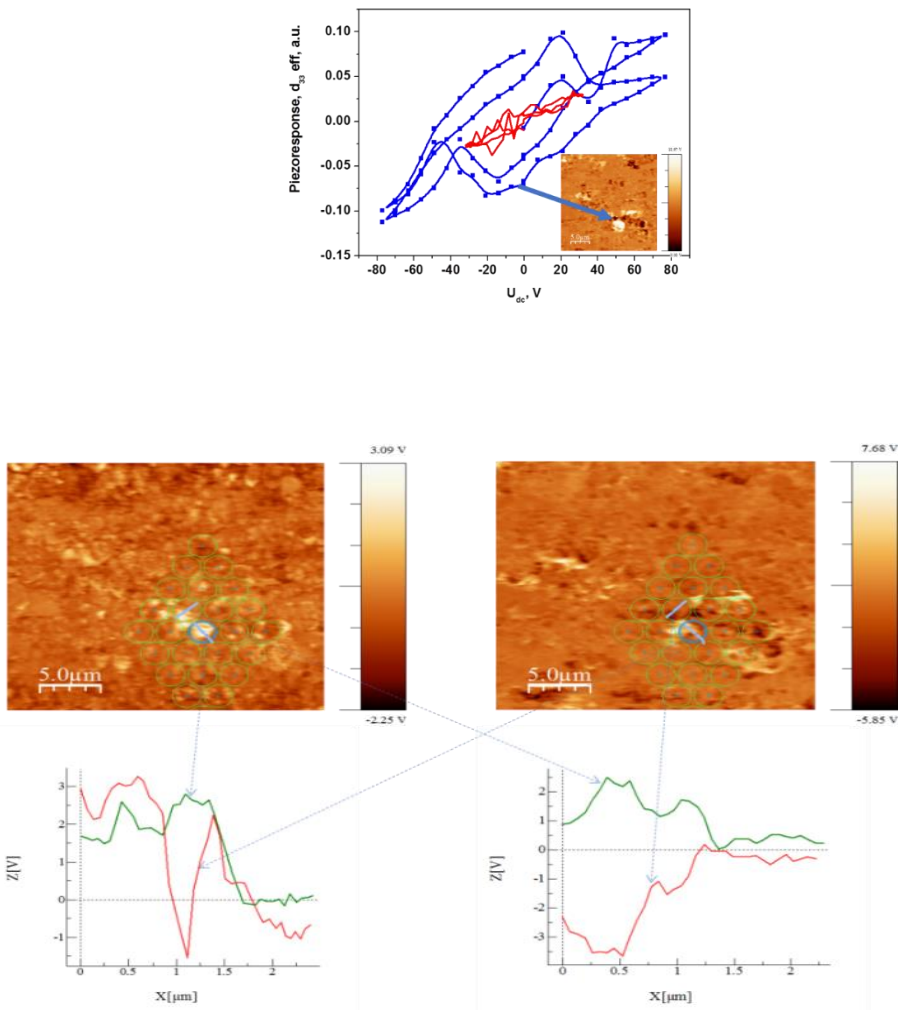

Figure 5.28 Switching results: a) hysteresis loop; and b) poling region and poling profile (green line before poling, red line after poling).

The remaining charges in the polymer and the polarization processes in the grain boundaries related by the dielectric behavior of the material could be acting as in opposition to the applied electric field by decreasing its effect in the sample. As the electric field is applied to the surface, it is dispersed in different directions and it might be not enough to polarize an effective area of the composite (Figure 5.29). It can also explain increase in loss factor (ε'') with the incorporation of NPs. Besides the behavior of the polymer related to charges in the surface there is an increase of energy losses under an applied field due to the contribution of different relaxation processes related before. The obtained results from PFM justify the obstacles to measure the piezoelectric properties of the films at macroscale.

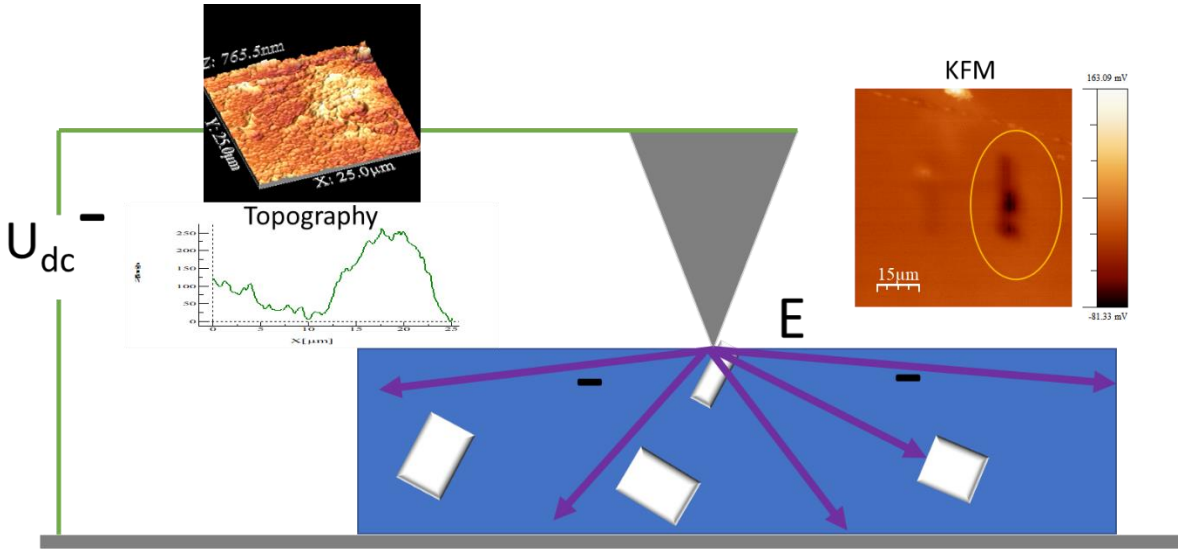

Figure 5.29 Possible behavior of the electric field while trying to do poling of the composite.

Chapter 6 Conclusion and future work

In this thesis, $BaTiO_3$ particles were synthesized by hydrothermal method at 200 °C using different reaction times. It was observed that the grain and crystallite size increase with reaction time. The XRD and Raman analyses showed that all particles are tetragonal at ambient temperature. The use of different precursors (hydrated and non-hydrated) not influenced the particles properties.

The particles synthetized over 24 h of reaction time were selected based on their size (around 300 nm), degree of tetragonality and reasonability of the duration of the synthesis reaction, to be used as fillers in a chitosan matrix. The particle size is important in the fabrication process as it could affect the homogeneity of the obtained composite[82]. Moreover, it is known that very small particles, prepared by hydrothermal method, may have their ferroelectric behavior compromised due to pseudo-tetragonality and large concentration of defects. Various concentrations of particles were tested in the preparation of the bionanocomposites. Freestanding about 50 μm thick films were obtained by solvent casting method and characterized to find their physical and dielectric properties. It was found that adding $BaTiO_3$ particles into the biopolymer improves the mechanical properties of the material, leading to a more resistant, flexible, and stretchable material. In addition, the films are also more resistant to water comparing to pure chitosan films, decreasing more than 60% of films solubility in water. This higher resistance could be related with the interaction of the $BaTiO_3$ particles with the chitosan structure. This is a favorable characteristic to enhance the durability of the material, when used for sensor or even for other biomedical applications. It is reported in literature that the wettedness of the skin at room temperature and air relative humidity between 60 and 80% is closed to 40%, being important the composite resistance[83].

Dielectric measurements were performed for samples with silver and gold electrodes. It was noted that gold electrodes were not continuous potentially due to the flexibility nature of the composite or to inadequate deposition conditions. Therefore, silver electrodes could be a better option to obtain more reliable information. The permittivity and dielectric loss of $BaTiO_3$–chitosan composites correlate well with a typical dielectric material. Impedance and conductivity also show behaviors that match with theoretical knowledge for this type of materials. The dielectric constant decreased with the increasing of frequency and $BaTiO_3$

ratio in the composite, whereas peaks of Tan delta were around 10 kHz and shifted to higher values for major concentration of $BaTiO_3$.

Corona poling was performed for 1:0.4, 1:0.8, 1:1.5 and 1:2 chitosan:$BaTiO_3$ samples without obtaining any result for d_{33} constant in the available equipment which only works at a fixed frequency (110 Hz). This situation leads to the attempt of finding piezoelectric response at local scale, using PFM technique. The bad hysteresis loop obtained for composite samples H_1:2 suggests lossy dielectrics behavior.

The PFM analysis showed the presence of piezoelectricity in the composite, therefore, the issues with poling at local scale could be related with the behavior of the biopolymer. The KPFM prove showed remaining charges in the chitosan films after applying an electric field, this behavior could be affecting the polarization at large scale of the film with nanoparticles as we could obtain switching in the microscale in zones where particles. The response to PFM technique also suggested that the bionanocomposite piezoelectric response could be dependent of frequency.

Overall, barium titanate nanoparticles with tetragonal phase could be produced using hydrothermal methodology, which is an environmentally friendly, using low energy consumption (200 C) and no organic solvents (water), and consequently at low cost. The incorporation of these nanoparticles into a chitosan matrix allows to produce films with high water and mechanical resistance, flexibility, and stretchability. These properties associated with the piezoelectricity of barium titanate nanoparticles allow to propose these bionanocomposites as a potential biocompatible material for biomedical devices. The sensor application, as the most innovative, is still needing further developments to improve the measurement capability and reduce the influence of the matrix on the piezoelectric and ferroelectric performance.

Future Work

Optimize the measurement process of chitosan-based films piezoelectric properties to reduce dielectric losses:

- Increase the electrode adherence to the biopolymer;
- Different electrode shapes (eg. ring) need to be tested;
- Study other setup to measure the piezoelectric response of the films at different frequencies and forces;
- Optimize the poling conditions for bionanocomposites.

To improve the piezoelectric properties of the films:

- Fabricate films with other type of biopolymer as alginate and starch, which have different structural characteristics in terms of the charge.
- Test the effect of particle size and of thermal treatment before particles dispersion into the polymer on the piezoelectric properties;
- PVDF could be test as a matrix since it is already known that it is a piezoelectric material.
- Study other processes to stabilize the films by for e.g. hot pressing after the film production, reticulation of chitosan polymeric chains and addition of carbon nanostructures .

The prototyping of a physical sensor could be done after improving the films in terms of ferroelectric properties.

References

[1] L. Play and B. Role, *Sensors in biomedical Applications*. 2000.

[2] T. Q. Trung and N. E. Lee, “Flexible and Stretchable Physical Sensor Integrated Platforms for Wearable Human-Activity Monitoringand Personal Healthcare,” *Adv. Mater.*, vol. 28, no. 22, pp. 4338–4372, 2016.

[3] P. M. Vilarinho, “Functional Materials: properties, processing and applications,” *Scanning Probe Microsc. Charact. Nanofabrication Device Appl. Funct. Mater.*, pp. 3–33, 2005.

[4] H. Wu, Y. Huang, F. Xu, Y. Duan, and Z. Yin, “Energy Harvesters for Wearable and Stretchable Electronics : From Flexibility to Stretchability,” *Adv. Mater.*, pp. 9881–9919, 2016.

[5] S. Zhao, J. Li, D. Cao, G. Zhang, J. Li, and K. Li, “Recent advancements in flexible and stretchable electrodes for electromechanical sensors : strategies , materials , and features,” 2017.

[6] S. R. Anton and H. A. Sodano, “A review of power harvesting using piezoelectric materials (2003 – 2006),” *SMart Mater. Struct.*, 2006.

[7] A. Singh, “Biomedical Sensing,” vol. 3, 2007, pp. 26–32.

[8] T. Yang, D. Xie, Z. Li, and H. Zhu, “Recent advances in wearable tactile sensors : Materials , sensing mechanisms , and device performance,” vol. 115, pp. 1–37, 2017.

[9] S. Priya, H. Song, Y. Zhou, R. Varghese, and A. Chopra, “A Review on Piezoelectric Energy Harvesting : Materials , Methods , and Circuits A Review on Piezoelectric Energy Harvesting : Materials , Methods , and Circuits,” no. February, 2017.

[10] J. A. Harvey and S. Williams, “Films, Coatings, Adhesives, Polymers, and Thermoelectric Materials,” in *Smart Materials*, 2008.

[11] M. Darder, P. Aranda, and E. Ruiz-Hitzky, “Bionanocomposites: A New Concept of Ecological, Bioinspired, and Functional Hybrid Materials,” *Adv. Mater.*, vol. 19, no. 10, pp. 1309–1319, 2007.

[12] G. Zhou, Y. Wang, and L. Cui, “Biomedical Sensor , Device and Measurement Systems,” 2015.

[13] P. Ripka and A. Tipek, *Modern Sensors Handbook*. 2010.

[14] S. W. Park, P. S. Das, and J. Y. Park, “Development of wearable and flexible insole type capacitive pressure sensor for continuous gait signal analysis,” *Org. Electron. physics, Mater. Appl.*, vol. 53, no. November 2017, pp. 213–220, 2018.

[15] S. Choi, H. Lee, R. Ghaffari, T. Hyeon, and D. H. Kim, “Recent Advances in Flexible and Stretchable Bio-Electronic Devices Integrated with Nanomaterials,” *Adv. Mater.*, vol. 28, no. 22, pp. 4203–4218, 2016.

[16] L. A. Kholkine, D. A. Kiselev, L. A. Kholkine, and A.safari, “Piezoelectric and Electrostrictive Ceramics Transducers and Generators.,” in *Smart Materials.*, 2008, p. 40.

[17] S. Rajala, S. Tuukkanen, and J. Halttunen, “Characteristics of piezoelectric polymer film sensors with solution-processable graphene-based electrode materials,” *IEEE Sens. J.*, vol. 15, no. 6, pp. 3102–3109, 2015.

[18] X. X. Gong, G. T. Fei, W. B. Fu, M. Fang, X. D. Gao, B. N. Zhong, and L. De Zhang, “Flexible strain sensor with high performance based on PANI/PDMS films,” *Org. Electron.*, vol. 47, pp. 51–56, 2017.

[19] S. Fuentes, J. Dubo, N. Barraza, R. González, and E. Veloso, “Hybrid chitosan-Pluronic F-127 films with BaTiO3:Co nanoparticles: Synthesis and properties,” *J. Magn. Magn. Mater.*, vol. 377, pp. 65–69, 2015.

[20] S. P. Priya, “Composite systems modeling-adptative structures: modeling and applications and hybrid composie«te,” 2008.

[21] L. Merhari, *Hybrid nanocomposites for nanotechonology (Electronic, optical, magnetic and biomedical applications)*. 2009.

[22] J. Gao, D. Xue, W. Liu, C. Zhou, and X. Ren, “Recent Progress on BaTiO3-Based Piezoelectric Ceramics for Actuator Applications,” *Actuators*, vol. 6, no. 3, p. 24, 2017.

[23] A. M. Neagu, L. Curecheriu, A. Cazacu, and L. Mitoseriu, “Impedance analysis and tunability of BaTiO3-chitosan composites: Towards active dielectrics for flexible electronics,” *Compos. Part B Eng.*, vol. 60, no. 4, pp. 515–530, 2014.

[24] E. Praveen, S. Murugan, and K. Jayakumar, “Investigations on the existence of piezoelectric property of a bio-polymer-chitosan and its application in vibration sensors,” *RSC Adv.*, vol. 7, no. 56, pp. 35490–35495, 2017.

[25] F. R. Fan, W. Tang, and Z. L. Wang, “Flexible Nanogenerators for Energy Harvesting and Self-Powered Electronics,” *Advanced Materials*. 2016.

[26] J. Lim, H. Jung, C. Baek, G. Hwang, and J. Ryu, “Nano Energy All-inkjet-printed fl exible piezoelectric generator made of solvent evaporation assisted BaTiO 3 hybrid material,” *Nano Energy*, vol. 41, no. July, pp. 337–343, 2017.

[27] M. Kriisa, E. Kärber, M. Krunks, V. Mikli, T. Unt, M. Kukk, and A. Mere, “Growth and properties of ZnO films on polymeric substrate by spray pyrolysis method,” *Thin Solid Films*, vol. 555, pp. 87–92, 2014.

[28] S. Murugan, D. Karthikesan, S. Sellathurai, E. Praveen, and K. Jayakumar, “Design of Mechanical Sensing System Based on Nano BaTiO3 Embedded in Biopolymer Electret,” in *Proceedings - 2014 5th International Symposium on Electronic System Design, ISED 2014*, 2014.

[29] Z. H. Lin, Y. Yang, J. M. Wu, Y. Liu, F. Zhang, and Z. L. Wang, “BaTiO3 nanotubes-based flexible and transparent nanogenerators,” *J. Phys. Chem. Lett.*, vol. 3, pp. 3599–3604, 2012.

[30] B. H. Fan, J. W. Zha, D. Wang, J. Zhao, and Z. M. Dang, “Size-dependent low-frequency dielectric properties in the BaTiO 3/poly(vinylidene fluoride) nanocomposite films,” *Appl. Phys. Lett.*, 2012.

[31] N. R. Alluri, S. Selvarajan, A. Chandrasekhar, B. Saravanakumar, J. H. Jeong, and S. J. Kim, “Piezoelectric BaTiO3/alginate spherical composite beads for energy harvesting and self-powered wearable flexion sensor,” *Compos. Sci. Technol.*, 2017.

[32] P. By, “Biomedical Sensor , Device and Measurement Systems,” *World ’ s Larg. Sci. , Technol. Med. Open Access B. Publ.*

[33] Radheshyam Rai, *Synthesis, Characterization & Application of Smart Materials*. 2012.

[34] G. G. Wallace and C. O. Too, “Smart Polymers for Biotechnology and Elastomers,” in *Smart Materials.*, 2008, p. 106.

[35] P. Salvo, V. Dini, F. Di Francesco, and M. Romanelli, “The role of biomedical sensors in wound healing,” vol. 8, pp. 15–18, 2015.

[36] J. E. Purdy, “Application of Smart Materials and Smart Structures to the Study of Aquatic Animals,” in *Smart Materials*, 2008.

[37] K. C. Kao, “Ferroelectrics, piezoelectrics, and pyroelectrics,” in *Dielectric Phenomena in Solids*, 2004, pp. 213–282.

[38] R. Zafar, K. Mahmood, S. Tabasum, F. Jabeen, and A. Noreen, “Polysaccharide based bionanocomposites , properties and applications : A review,” *Int. J. Biol. Macromol.*, vol. 92, pp. 1012–1024, 2016.

[39] vazhiyil Venugopal, *Marine Polysaccharides*. 2011.

[40] W. Suginta, P. Khunkaewla, and A. Schulte, “Electrochemical biosensor applications of polysaccharides chitin and chitosan,” *Chem. Rev.*, vol. 113, no. 7, pp. 5458–5479, 2013.

[41] C. Gels, “Chitosan-Based Gels and Hydrogels,” in *Smart Materials*, 2008.

[42] J. P. Fisher, A. G. Mikos, and J. D. Bronzino, *Tissue engineering*. 2007.

[43] S. T. Koev, P. H. Dykstra, X. Luo, G. W. Rubloff, W. E. Bentley, G. F. Payne, and R. Ghodssi, “Chitosan: an integrative biomaterial for lab-on-a-chip devices,” *Lab Chip*, 2010.

[44] K. Uchino, *The development of piezoelectric materials and the new perspective*, no. January. 2010.

[45] K. Uchino, *Ferroelectric Devices*. 2000.

[46] G. H. Haertling, “Ferroelectric Cramics: History and Technology,” *J. Am. Ceram. Soc.*, vol. 82, pp. 797–818, 1999.

[47] Pblittlewood, “Physics of ferroelectrics.” 2002.

[48] M. M. Vijatovi, J. D. Bobi, and B. D. Stojanovi, “History and Challenges of Barium Titanate : Part I,” vol. 40, pp. 155–165, 2008.

[49] R. W. Rice, *Mechanical properties of ceramics and composites*. 2000.

[50] A. Nathan, A. Ahnood, M. T. Cole, S. Lee, Y. Suzuki, P. Hiralal, F. Bonaccorso, T. Hasan, L. Garcia-Gancedo, A. Dyadyusha, S. Haque, P. Andrew, S. Hofmann, J. Moultrie, D. Chu, A. J. Flewitt, A. C. Ferrari, M. J. Kelly, J. Robertson, G. A. J. Amaratunga, and W. I. Milne, “Flexible electronics: The next ubiquitous platform,” *Proceedings of the IEEE*, 2012.

[51] R. E. Riman and Wojciech L.Suchanek, “Intelligent synthesis of Smart Ceramic Materials,” in *Smart materials*, 2008, p. 71.

[52] C. Perdomo fernandez, E. Rivera Figueroa, and J. Rodriguez Paez, “BaTiO3 Obtained by coprecipitation method,” *Dyna*, vol. 146, pp. 223–230, 2008.

[53] F. Maxim, P. Ferreira, P. M. Vilarinho, and I. Reaney, “Hydrothermal synthesis and crystal growth studies of BaTiO3 using Ti nanotube precursors,” *Cryst. Growth Des.*, vol. 8, no. 9, pp. 3309–3315, 2008.

[54] B. Jaffe, W. R. Cook Jr., and H. Jaffe, *Piezoelectric Ceramics*, vol. 3. 1971.

[55] H. Chen and Y. Chen, “Hydrothermal Synthesis of Barium Titanate,” no. 300 mL, pp. 473–483, 2003.

[56] H. Zarkoob, S. Ziaei-Rad, M. Fathi, and H. Dadkhah, “Synthesis, characterization and bioactivity evaluation of porous barium titanate with nanostructured hydroxyapatite coating for biomedical application,” *Adv. Eng. Mater.*, vol. 14, no. 6, pp. 322–329, 2012.

[57] A. Prasad, M. R. Sankar, and V. Katiyar, “State of Art on Solvent Casting Particulate Leaching Method for Orthopedic ScaffoldsFabrication,” *Mater. Today Proc.*, vol. 4, pp. 898–907, 2017.

[58] A. S. Ferreira, C. Nunes, A. Castro, P. Ferreira, and M. A. Coimbra, “Influence of grape pomace extract incorporation on chitosan films properties,” *Carbohydr. Polym.*, vol. 113, pp. 490–499, 2014.

[59] H. L. W. Chan, M. C. Cheung, and C. L. Choy, “Study on BaTiO 3 / P (VDF-TrFE) 0 – 3 composites,” vol. 0193, no. 1999, pp. 0–3, 2011.

[60] R. C. Alkire, D. M. Kolb, J. Lipkowski, and P. N. Ross, *Advances in electrochemical science and engineering*, vol. 13. 2013.

[61] C. . Silva, C. G. A. Lima, A. G. Pinheiro, J. C. Góes, S. D. Figueiro, and A. S. B. Sombrab, “On the piezoelectricity of collagen-chitosan films,” pp. 4–6, 2001.

[62] C. G. A. Lima, R. S. de Oliveira, S. D. Figueiró, C. F. Wehmann, J. C. Góes, and A. S. B. Sombra, “DC conductivity and dielectric permittivity of collagen-chitosan films,” *Mater. Chem. Phys.*, vol. 99, no. 2–3, pp. 284–288, 2006.

[63] S. D. Jang, J. H. Kim, C. Zhijiang, and J. Kim, “The effect of chitosan concentration on the electrical property of chitosan-blended cellulose electroactive paper,” *Smart Mater. Struct.*, vol. 18, no. 1, pp. 1–6, 2009.

[64] Z. Cai and J. Kim, “Characterization and electromechanical performance of cellulose-chitosan blend electro-active paper,” *Smart Mater. Struct.*, vol. 17, no. 3, 2008.

[65] S. Rajala, T. Siponkoski, E. Sarlin, M. Mettänen, M. Vuoriluoto, A. Pammo, J. Juuti, O. J. Rojas, S. Franssila, and S. Tuukkanen, “Cellulose Nanofibril Film as a Piezoelectric Sensor Material,” *ACS Appl. Mater. Interfaces*, 2016.

[66] A. Hänninen, E. Sarlin, I. Lyyra, T. Salpavaara, M. Kellomäki, and S. Tuukkanen, “Nanocellulose and chitosan based films as low cost, green piezoelectric materials,” *Carbohydr. Polym.*, vol. 202, no. September, pp. 418–424, 2018.

[67] E. Praveen, S. Murugan, K. Jayakumar, E. Praveen, S. Murugan, and K. Jayakumar, “Nano ZnO Embedded in Chitosan Matrix for Vibration Sensor Application,” vol. 050032, no. 2015, 2015.

[68] Y. Zhao, Q. Liao, G. Zhang, Z. Zhang, Q. Liang, X. Liao, and Y. Zhang, “High output piezoelectric nanocomposite generators composed of oriented BaTiO3 NPs at PVDF,” *Nano Energy*, vol. 11, pp. 719–727, 2014.

[69] S. Singh, S. S. Dey, S. Singh, and N. Kumar, “ScienceDirect Preparation and Characterization of Barium Titanate Composite Film,” *Mater. Today Proc.*, vol. 4, no. 2, pp. 3300–3307, 2017.

[70] K. S. Ramadam, D. Sameoto, and S. Evoy, “A review of piezoelectric polymers as functional materials for electromechanical transducers,” 2014.

[71] W. S. Rasband and U. U. S. National Institutes of Health, Bethesda, Maryland, “Image J.” 1997.

[72] S. Siddiqui, D. Kim, L. Thai, and M. Triet, “High-performance flexible lead-free nanocomposite piezoelectric nanogenerator for biomechanical energy harvesting and storage,” pp. 177–185, 2015.

[73] N. Rodríguez, A. Valderrama, H. Alarcón, and A. López, “Preparación de partículas de quitosano reticuladas con tripolifosfato y modificadas con polietilenglicol,” *Rev Soc Quím Perú*, vol. 76, no. 4, pp. 336–354, 2010.

[74] “The C = O stretching frequency aldehydes and ketones A summary of the principle infrared bands and their assignments .” .

[75] A. Baranwal, A. Kumar, A. Priyadharshini, G. S. Oggu, I. Bhatnagar, A. Srivastava, and P. Chandra, *Chitosan: An undisputed bio-fabrication material for tissue engineering and bio-sensing applications*. Elsevier B.V., 2018.

[76] A. Hänninen, S. Rajala, T. Salpavaara, M. Kellomäki, and S. Tuukkanen, “Piezoelectric Sensitivity of a Layered Film of Chitosan and Cellulose Nanocrystals,” *Procedia Eng.*, vol. 168, pp. 1176–1179, 2016.

[77] S. M. Ojagh, M. Rezaei, S. H. Razavi, and S. M. H. Hosseini, “Development and evaluation of a novel biodegradable film made from chitosan and cinnamon essential oil with low affinity toward water,” *Food Chem.*, vol. 122, no. 1, pp. 161–166, 2010.

[78] R. Allemang, J. De Clerck, C. Niezrecki, and A. Wicks, “Chapter 16:Composites,” in *Material science and engineering introduction*, pp. 577–617.

[79] S. Nayak, T. K. Chaki, and D. Khastgir, “Development of Flexible Piezoelectric Poly (dimethylsiloxane) − BaTiO 3 Nanocomposites for Electrical Energy Harvesting,” 2014.

[80] Q. Wang, C. Liu, Y. Gao, Y. Ma, Y. Han, and C. Gao, “Mixed conduction and grain boundary effect in lithium niobate under high pressure,” *Appl. Phys. Lett.*, vol. 106, no. 13, pp. 1–6, 2015.

[81] R. Rianyoi, R. Potong, N. Jaitanong, R. Yimnirun, and A. Chaipanich, “Dielectric, ferroelectric and piezoelectric properties of 0-3 barium titanate-Portland cement composites,” *Appl. Phys. A Mater. Sci. Process.*, vol. 104, no. 2, pp. 661–666, 2011.

[82] C. O. Blattmann and S. E. Pratsinis, “Nanoparticle Filler Content and Shape in Polymer Nanocomposites †,” no. August, pp. 1–30, 2018.

[83] R. H. Mole, “The relative humidity of the skin,” *J-Physiol*, vol. I07, pp. 399–411, 1948.

APPENDIX

Tabla 1. Measured parameters for samples of $BaTiO_3$-Chitosan films.

sample	*Thickness (µm)*	*density (g/cm^3)*	*Moisture content (%)*	*water solubility (%)*	*contact angle (θ)*		*young modulus (MPa)*	*tensile strength (MPa)*	*Elongation (%)*	*Au- εr (1kHz)*	*C (pF)*	*Au-Tan δ*	*Ag- εr (1kHz)*	*C (pF)*	*Ag-Tan δ*
					TOP	*BOTTOM*									
C	46,2	1,3	28	38	112	112	220	12	26	819	4438	2,51	397	2149	0,34
H_1:0.4	56,8	1,34	21	31	107	105	218	12	24	1700	7493	1,71	668	2946	0,55
H_1:0.5	49	1,38	18	29	109	107	443	15	21	1143	5840	2,23	631	3224	0,53
H_1:0.6	45,3	1,47	16	27	108	104	575	25	33	953	5267	1,92	694	3833	0,56
H_1:0.8	49	1,57	13	18	108	103	230	26	44	1165	5952	2,28	703	3593	0,63
H_1:1.5	49,9	1,54	10	15	108	94	127	23	47	1557	7811	2,19	1266	6353	0,77
H_1:2	52,6	2,01	7	12	108	94	168	28	49	923	4393	2,33	750	3572	0,72